



On the size-dependent bending and buckling of the partially covered laminated microplate

Guangyang Fu^{1,2} · Zhenjie Zhang³ · Yulin Ma^{1,2} · Hongyu Zheng^{1,2} · Qianjian Guo¹ · Xuye Zhuang¹

Received: 8 October 2021 / Accepted: 6 April 2022

© The Author(s), under exclusive licence to Springer-Verlag London Ltd., part of Springer Nature 2022

Abstract

The bending and buckling of the microcomponents show size dependency. The strain gradient elasticity theory is proposed to explain the size dependency. In this paper, we derive the theoretical relations among the modified strain gradient elasticity theory, the modified couple stress theory and the general strain gradient elasticity theory, and clarify the degradation relation. The general theory includes all strain gradients while the modified strain gradient elasticity theory and the modified couple stress theory only contain part of strain gradients. By ignoring the deviatoric part of the strain gradients $\eta_{ijk}^{(2)}$ or the symmetric part of the strain gradients η_{ijk}^s , the general theory is simplified as the modified couple stress theory or the modified strain gradient elasticity theory, respectively. The ability of the general theory and the reduced theories in describing the bending and buckling response of the partially covered laminated microplate is subsequently compared. Results reveal that the general theory predicts smaller bending deflection and axial displacement while larger buckling load than that of the reduced theories. The general theory is more effective in reflecting the size effects. In addition, it is found that the increase of the thickness or radius of the upper elastic layer makes the buckling load increase while the deflection increase firstly and then decrease. There exists the specific radius ratio and thickness ratio to make the clamped-clamped microplate achieve the maximum deflection.

✉ Hongyu Zheng
zhenghongyu@sdut.edu.cn

✉ Qianjian Guo
guoqianjian@163.com

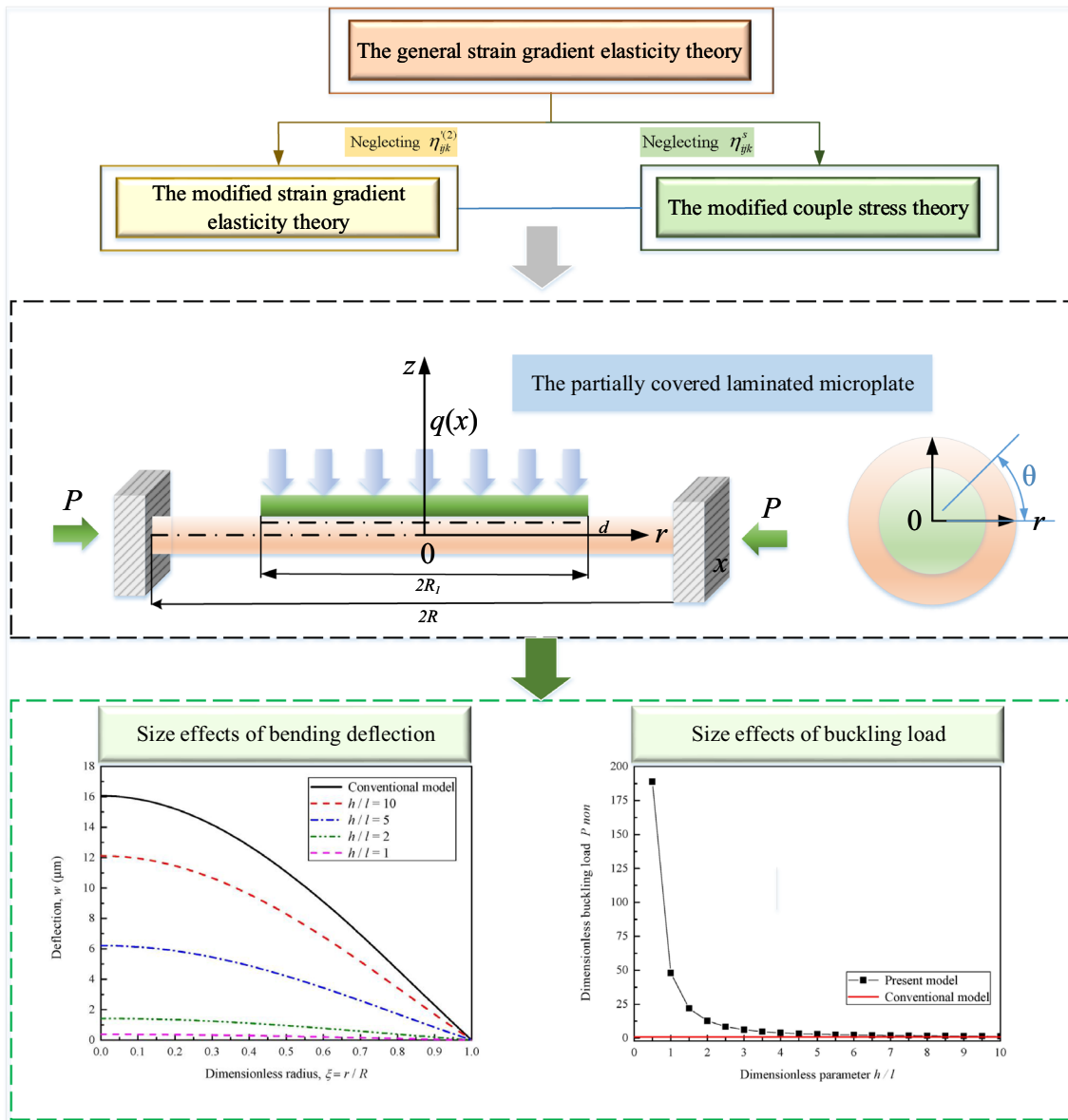
✉ Xuye Zhuang
zxye8888@163.com

¹ Centre for Advanced Laser Manufacturing (CALM),
School of Mechanical Engineering, Shandong
University of Technology, Zibo 255000, Shandong,
People's Republic of China

² State Key Laboratory of Applied Optics, Changchun
Institute of Optics, Fine Mechanics and Physics, Chinese
Academy of Sciences, Changchun 130033, Jilin,
People's Republic of China

³ School of Mechanical Engineering, Shandong University,
Jinan 250061, Shandong, People's Republic of China

Graphical abstract



Keywords Size dependency · Bending · Buckling · Laminated microplate

1 Introduction

The partially covered laminated plate constitutes the functional component of the pump [1], energy harvester [2] and acoustic sensor [3]. The performance of the devices is determined by the mechanical property of the plate. In order to accurately describe the pump flow, energy conversion and dynamic density of the devices, more and more attentions have been paid to the mechanical analysis of the plate.

For the static bending of the macroplate, the static deflection of the partially covered laminated plate was derived by Afzal [4] using the classical theory. Nguyen et al. [5] performed the static analysis of the partially covered plate actuator with various design parameters. Prasad et al. [6] further considered the effects from the variation of the location of the upper layer on the bending behaviour of the plate. Bakhtriari-Shahri and Moeenfarid [7] performed the bending and vibration simulation of the plate and optimized the structure parameters. Based on the bending model above, Wang et al.

[8] subsequently designed the valveless pump and calibrated the performance of the pump. For the dynamic vibration of the macroplate, Shahri and Moeenfarid [9] studied the random vibration response of the plate and determined the vibration frequency. Kan et al. [10] established the theoretical model for the hydraulic actuator, and further determined the optimal frequency for drug delivery. The nonlinear bending response of the plate with various boundary conditions was solved by Hu et al. [11]. Yuan et al. [12] further analysed the softening and hardening characteristics of the nonlinear vibration response. Sahoo and Ray [13] performed the nonlinear dynamic analysis of the laminated plate integrated with rectangular pitch and elliptical pitch, and found that compared with the rectangular pitch, the elliptical pitch is more effective in attenuating the vibration. Based on the vibration model above, Sun et al. [14] subsequently designed the wind-based vibration energy harvester with the vortex effects. Chong and Williams [15] further considered the magnetoelectric effects when they performed the vibration analysis of the plate.

The above models about the linear and nonlinear bending and vibration responses of the partially covered laminated macroplate are applied to characterize the mechanical response of the microplate. Microplate is not only the miniaturization of the macroplate. The mechanical property of the microplate is obvious different from those of the macroplate. The variation of the bending rigidity, dynamic vibration and buckling load depends on the feature size of the microplate [16–18] and thus shows size dependency obviously. However, classical theory is unable to capture the size dependency.

The rotation gradients were originally considered as the reason for the size effects. The classical couple stress theory [19, 20] was applied widely to describe the effects from rotation gradients. Subsequently, the modified versions [21–23] were also proposed. However, the rotation gradients were proved to be part of the strain gradients [24]. Neff et al. [25, 26] further proved the limitations of the application of the modified versions. To include the effects from all strain gradients, Mindlin and Eshel [24, 27] firstly established the theoretical framework of the general strain gradient elasticity theory with five length parameters. For simplification of the general theory, the modified strain gradient elasticity theories were proposed [16, 28, 30, 31]. Recently, Zhou et al. [29] proved the number of the independent length parameters is three, reformulated the general theory, and proposed the general theory with three independent length parameters. The differences among these theories in describing the size-dependent buckling response of the partially covered laminated microbeam were further confirmed [32].

For the static bending of the monolayer microplate, Yue et al. [33] performed the bending analysis of the microplate. The effects of various loading and boundary conditions on

the bending deflection were discussed by Barretta et al. [34]. The solution was subsequently extended to the incompressible functionally graded plates [35]. Thai et al. [36] performed the bending analysis of the carbon nanotube-reinforced plate. The similar method was also applied by Akgöz and Civalek [37, 38] to analyse the size-dependent mechanical responses of the microcomponents. Subsequently, the effects from the nonlocal elasticity and rotation gradients were also explored by Civalek et al. [39] using the Chebyshev-Ritz method. Farzam and Hassani [40] further considered the temperature effects. For the dynamical vibration of the monolayer microplate, Shahrabaki [41] performed the vibration analysis of the plate with various boundary conditions. Alizadeh and Fattahi [42] further extended the solution to the functionally graded microplate. Afterwards, this solution was extended to dynamic analysis of the plate supported by the winkler foundation [43]. Nguyen et al. [44] further solved the vibration problem of the cracked functionally graded microplates and discussed the effects of the location of the crack on the vibration frequency. The vibration behaviour of the plate with internal hinges was subsequently solved [45]. Thanh et al. [46] and Li et al. [47] performed the nonlinear bending and vibration analysis of the plate, respectively. For the buckling response of the monolayer microplate, Zhou et al. [48] performed the buckling analysis of the plate. Akgöz and Civalek [49] proposed a microstructure-dependent sinusoidal plate model with strain gradients, and solved the buckling problem. Ullah et al. [50] further considered the influences from boundary conditions when they solved the buckling problem. The solution was subsequently extended to the functionally graded microplate [51]. The buckling problem of the plate with the porosity effects and thermal effects was also solved [52]. Tenenbaum et al. [53] performed the buckling analysis of the corner supported orthotropic microplate.

For the static bending of the bilayer microplate, Arefi et al. [54] performed the bending analysis of the plate with various loading conditions. The bending behaviour of the microplate under double sinusoidal loading was subsequently solved [55]. Ghorbanpour and Zamani [56] extended the solution to the functionally graded plate. Gao and Sun [57] subsequently solved the nonlinear bending problem. The influence from the magnetic field on the bending deflection was further considered [58]. For the dynamical vibration of the bilayer microplate, Zhang et al. [61] compared the effects of loading and boundary conditions on the vibration of orthotropic bilayer plates. Nguyen et al. [62] extended the solution to the functional gradient microplate. The influence of nonlinear effects on the vibration behaviour of the plate was analysed by Roque et al. [63]. Zuo et al. [64] further considered the thermoelastic damping effects. The linear and nonlinear analysis of the vibration of the plate were also performed [65]. For the buckling response of the bilayer

microplate, Reddy et al. [66] performed the uniaxial and biaxial buckling analysis of the plate. Afterwards, Mondal et al. [67] further considered the nonlinear effects and thermal effects. The nonlinear buckling analysis of the microplate with different boundary conditions was subsequently performed by Magnucki et al. [68]. Arefi et al. [69] further considered the influence from the temperature. The influence from the magnetic field on the buckling load was subsequently solved [58].

Although much attention has been paid to the mechanical response of microplate, the size dependency of the same microplate predicted by different strain gradient theories is different. In addition, little attention is focused on the bending and buckling behaviour of the partially covered laminated microplate, while the plate of this type is usually served as the key functional components in the micro-devices. To reasonably estimate the size effects of the mechanical responses of the microplate, and offer a theoretical basis for the structure design and performance optimization of the micro-devices, it is urgent to clarify the relations between the general theory and other strain gradient theories, and further apply the general theory to perform the buckling and bending analysis of the partially covered laminated microplate.

To fill in the gaps, this paper discusses the differences between the general theory and other strain gradient theories in detail, and presents the corresponding degradation relation, then, the partially covered laminated microplate model with strain gradient effects is established using the general strain gradient theory [29]. The bending and buckling analysis of the laminated plate under various boundary conditions are performed.

The size dependency of the bending deflection and buckling load are discussed.

The paper is organized as follows.

The equations of the general strain gradient theory are reviewed in Sect. 2. The mechanical response model of the laminated plate is derived in Sect. 3. Subsequently, we perform the bending and buckling analysis of the laminated plate in the Sects. 4 and 5, respectively. Subsequently, the size dependency of bending and buckling responses of the plate are studied. Finally, the conclusion is given in Sect. 6.

2 Theoretical comparison

2.1 Strain gradient elasticity theory

The strain gradient elasticity theory considers the influence from the strain and strain gradients, and thus the strain energy density is expressed as

$$w = w(\varepsilon_{ij}, \eta_{ijk}) \quad (1)$$

where the strain tensor ε_{ij} is written as

$$\varepsilon_{ij} = \frac{1}{2}(u_{i,j} + u_{j,i}) \quad (2)$$

the strain gradient tensor η_{ijk} is written as

$$\eta_{ijk} = \varepsilon_{jk,i} \quad (3)$$

For isotropic material, Mindlin and Eshel [27] firstly given the general expression of the strain energy density of Eq.(1) as

$$\begin{aligned} w = & \frac{1}{2} \lambda \varepsilon_{ii} \varepsilon_{jj} + \mu \varepsilon_{ij} \varepsilon_{ij} + a_1 \eta_{iik} \eta_{kij} + a_2 \eta_{ijj} \eta_{ikk} \\ & + a_3 \eta_{iik} \eta_{jjk} + a_4 \eta_{ijk} \eta_{ijk} \\ & + a_5 \eta_{ijk} \eta_{kji} \end{aligned} \quad (4)$$

where μ and λ are the Lamé constants. a_n ($n = 1, 2, 3, 4, 5$) are the material constants.

The strain gradient tensor η_{ijk} can be expressed in the form of the anti-symmetric splitting and symmetric splitting as

$$\eta_{ijk} = \eta_{ijk}^s + \eta_{ijk}^a = \eta_{ijk}^{(0)} + \eta_{ijk}^{(1)} + \eta_{ijk}^{as} + \eta_{ijk}^{aa} \quad (5)$$

where $\eta_{ijk}^{(1)}$ and $\eta_{ijk}^{(0)}$ are, respectively, the traceless and trace parts of the symmetric strain gradient tensor η_{ijk}^s . η_{ijk}^{as} and η_{ijk}^{aa} are respectively the symmetric and anti-symmetric parts of the anti-symmetric strain gradient tensor η_{ijk}^a .

The strain gradient tensor η_{ijk} can also be expressed in the form of the deviatoric splitting and hydrostatic splitting as

$$\eta_{ijk} = \eta_{ijk}^h + \eta_{ijk}^{(1)} + \eta_{ijk}^{as} + \eta_{ijk}'^{(2)} \quad (6)$$

where η_{ijk}^h is the hydrostatic part of the strain gradient tensor. $\eta_{ijk}'^{(2)}$ is the deviatoric part of the strain gradient tensor.

Using the anti-symmetric splitting and symmetric splitting, deviatoric splitting and hydrostatic splitting, Zhou et al. [29] reformulated the general theory [27], proved the number of the independent material parameters is three, and given the strain energy density as

$$\begin{aligned} w_0 = & \frac{1}{2} \lambda \varepsilon_{ii} \varepsilon_{jj} + \mu \varepsilon_{ij} \varepsilon_{ij} + \left(\frac{9}{5} \mu l_0^2 - \frac{4}{15} \mu l_1^2 - \mu l_2^2 \right) \eta_{iik} \eta_{kij} \\ & - \left(\frac{6}{5} \mu l_0^2 + \frac{4}{15} \mu l_1^2 - 2 \mu l_2^2 \right) \eta_{iik} \eta_{kji} \\ & + \left(\frac{6}{5} \mu l_0^2 - \frac{1}{15} \mu l_1^2 - \mu l_2^2 \right) \eta_{kii} \eta_{kjj} \\ & + \left(\frac{1}{3} \mu l_1^2 + 2 \mu l_2^2 \right) \eta_{ijk} \eta_{ijk} + \left(\frac{2}{3} \mu l_1^2 - 2 \mu l_2^2 \right) \eta_{kij} \eta_{ijk} \end{aligned} \quad (7)$$

The strain energy density in Eq. (7) can also be expressed in the form of the strain gradient components as

$$w_0 = \frac{1}{2} \lambda \varepsilon_{ii} \varepsilon_{jj} + \mu \varepsilon_{ij} \varepsilon_{ij} + 3\mu l_0^2 \left(\eta_{ijk}^{(0)} \eta_{ijk}^{(0)} + \eta_{ijk}^{aa} \eta_{ijk}^{aa} \right) + \mu l_1^2 \eta_{ijk}^{(1)} \eta_{ijk}^{(1)} + 3\mu l_2^2 \eta_{ijk}^{as} \eta_{ijk}^{as} \tag{8}$$

$$w_0 = \frac{1}{2} \lambda \varepsilon_{ii} \varepsilon_{jj} + \mu \varepsilon_{ij} \varepsilon_{ij} + 3\mu l_0^2 \left(\eta_{ijk}^h \eta_{ijk}^h + \eta_{ijk}^{\prime(2)} \eta_{ijk}^{\prime(2)} \right) + \mu l_1^2 \eta_{ijk}^{(1)} \eta_{ijk}^{(1)} + 3\mu l_2^2 \eta_{ijk}^{as} \eta_{ijk}^{as} \tag{9}$$

In which l_0, l_1 and l_2 represent the length parameters.

2.2 Relation to the other strain gradient elasticity theory

Various strain gradient elasticity theories including the modified strain gradient elasticity theory [16] and the modified couple stress theory [21] were proposed to capture size effects. Here, we will discuss the reduction relation among the modified strain gradient elasticity theory, the general theory and the modified couple stress theory.

The modified strain gradient elasticity theory [16] includes the dilatation gradients, the deviatoric stretch gradients, the classical strain and the symmetric rotational gradients. To derive the theoretical relations between the general theory and the modified strain gradient elasticity theory, the strain energy density of the general theory is expressed in the form of the hydrostatic and deviatoric splitting (Eq. 9). By ignoring the contributions from the deviatoric part of the strain gradients $\eta_{ijk}^{\prime(2)}$, the following equation is obtained as

$$w_0 = \frac{1}{2} \lambda \varepsilon_{ii} \varepsilon_{jj} + \mu \varepsilon_{ij} \varepsilon_{ij} + 3\mu l_0^2 \eta_{ijk}^h \eta_{ijk}^h + \mu l_1^2 \eta_{ijk}^{(1)} \eta_{ijk}^{(1)} + 3\mu l_2^2 \eta_{ijk}^{as} \eta_{ijk}^{as} \tag{10}$$

The relation between the strain gradients and the rotational gradients is given as

$$\eta_{ijk}^{as} = \frac{1}{3} \left(e_{ijp} \chi_{pk}^s + e_{ikp} \chi_{pj}^s \right) \tag{11}$$

$$\eta_{ijk}^{aa} = \frac{1}{3} \left(e_{ijp} \chi_{pk}^a + e_{ikp} \chi_{pj}^a \right)$$

with

$$\chi_{ij}^s = \frac{1}{2} \left(e_{ipq} \varepsilon_{qj,p} + e_{jpq} \varepsilon_{qi,p} \right) \tag{12}$$

$$\chi_{ij}^a = \frac{1}{2} \left(e_{jpq} \varepsilon_{qi,p} - e_{ipq} \varepsilon_{qj,p} \right)$$

where χ_{ij}^s and χ_{ij}^a are respectively the symmetric and anti-symmetric parts of the rotational gradients χ_{ij} .

Using Eqs. (10) and (11), the strain energy density for the modified strain gradient elasticity theory is obtained as

$$w_0 = \frac{1}{2} \lambda \varepsilon_{ii} \varepsilon_{jj} + \mu \varepsilon_{ij} \varepsilon_{ij} + \mu l_3^2 \varepsilon_{nm,i} \varepsilon_{nm,i} + \mu l_4^2 \eta_{ijk}^{(1)} \eta_{ijk}^{(1)} + \mu l_5^2 \chi_{pi}^s \chi_{pi}^s \tag{13}$$

with

$$l_3 = l_0 \quad l_4 = l_1 \quad l_5 = \sqrt{2} l_2 \tag{14}$$

The modified couple stress theory [21] contains the effects only from the symmetric part of the rotational gradients. It can be seen from Eq. (11) that the symmetric part of the rotational gradients is related to the symmetric part of the anti-symmetric strain gradients. Therefore, to derive the theoretical relations between the modified couple stress theory and the general theory, the strain energy density of the general theory is expressed in the form of the symmetric and anti-symmetric splitting (Eq. 8).

By ignoring the contributions from symmetric strain gradients $\eta_{ijk}^{(0)}$ and $\eta_{ijk}^{(1)}$, the anti-symmetric part of the anti-symmetric strain gradients η_{ijk}^{aa} , and using Eq. (8), the modified couple stress theory strain energy density is obtained as

$$w_0 = \frac{1}{2} \lambda \varepsilon_{ii} \varepsilon_{jj} + \mu \varepsilon_{ij} \varepsilon_{ij} + \mu l_5^2 \chi_{pi}^s \chi_{pi}^s \tag{15}$$

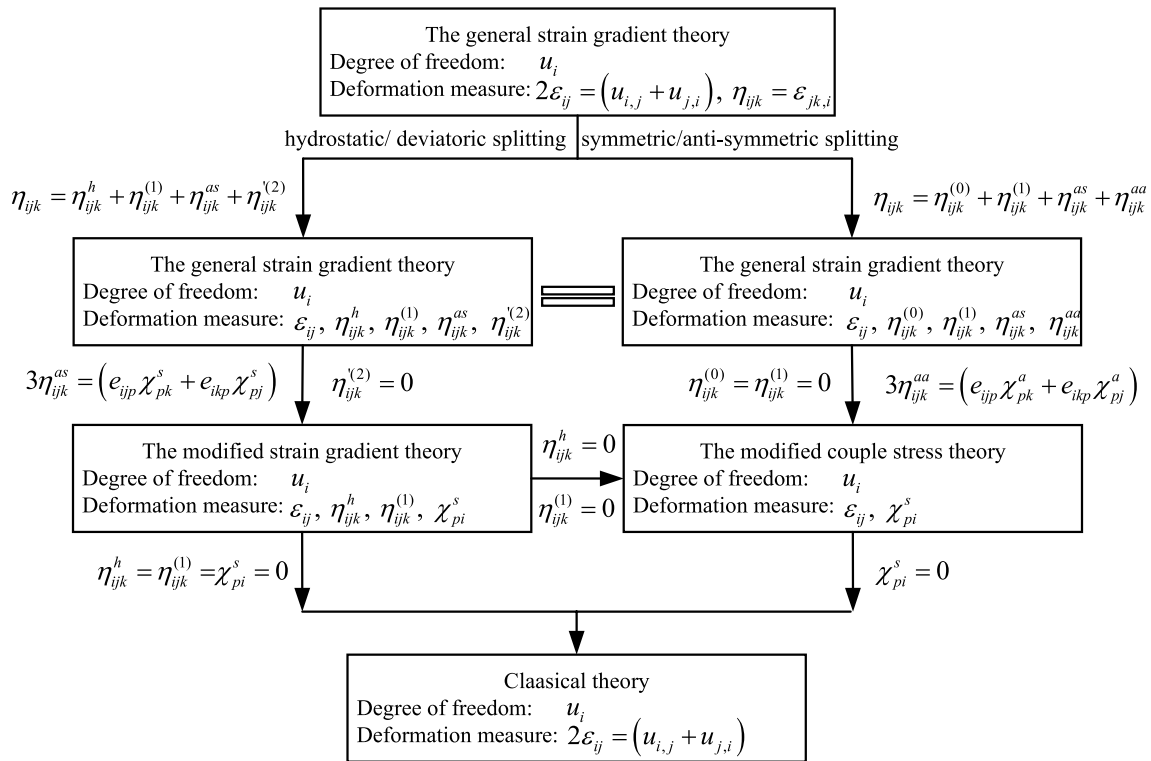
From Eqs. (9)–(13), (8), (11) and (15), it can be seen that the general theory can be simplified as the modified couple stress theory or the modified strain gradient elasticity theory respectively by ignoring the contribution from the symmetric part of the strain gradients η_{ijk}^s or the deviatoric part of the strain gradients $\eta_{ijk}^{\prime(2)}$. The differences and relations among the strain gradient theories are summarized in Table 1.

3 Size-dependent model for Kirchhoff plate

The isotropic homogeneous partially covered laminated circular microplate subjected to the transverse load $q(r, \theta)$ and the axial compressive force P is shown in Fig. 1. The contact of the upper and lower elastic layer is assumed to be ideal. Here, we adopt the cylindrical coordinate system. The $r - \theta$ plane is at the centroid surface of the lower microplate. The thickness of the lower and upper circular microplate are respectively defined as h_1 and h_2 . The radius of the lower and upper circular microplate are defined as R and R_1 , respectively.

Due to the geometric discontinuity of the circular microplate, the neutral surface of the circular microplate is piecewise [59, 60]. The neutral surface of the circular microplate ($R_1 < r < R$) lies along the centroid surface of the lower

Table 1 The contacts among the strain gradient theories



microplate. The location of the neutral surface of the circular microplate ($0 < r < R_1$) is unknown, and assumed to be d away from the centroid surface of the lower circular microplate. Each region of the circular microplate is separately modelled as the Kirchhoff circular microplate. The displacement model of the circular microplate is given as

$$\begin{aligned}
 u_{r1} &= -z \frac{\partial w(r)}{\partial r} & u_{\theta 1} &= 0 & u_{z1} &= w(r) & R_1 < x < R \\
 u_{r2} &= -(z + d) \frac{\partial w(r)}{\partial r} & u_{\theta 2} &= 0 & u_{z2} &= w(r) & 0 < x < R_1
 \end{aligned}
 \tag{16}$$

In Eq. (16), u_{ri} , $u_{\theta i}$ and u_{zi} ($i = 1, 2$) are the r, θ and z direction displacement components, respectively. The lateral deflection is denoted as $w(x)$.

Based on Eqs. (2), (3) and (16), the non-laminated region non-zero strain and strain gradient are, respectively, written as

$$\begin{aligned}
 \epsilon_{rr} &= -z \frac{\partial^2 w}{\partial r^2} & \epsilon_{\theta\theta} &= -z \frac{\partial^2 w}{r \partial r} \\
 \eta_{rrr} &= -z \frac{\partial^3 w}{\partial r^3} & \eta_{zrr} &= -\frac{\partial^2 w}{\partial r^2} & \eta_{z\theta\theta} &= -\frac{1}{r} \frac{\partial w}{\partial r} \\
 \eta_{\theta\theta r} &= -z \frac{1}{r} \frac{\partial^2 w}{\partial r^2} + \frac{1}{r^2} z \frac{\partial w}{\partial r} \\
 \eta_{r\theta\theta} &= -z \frac{1}{r} \frac{\partial^2 w}{\partial r^2} + \frac{1}{r^2} z \frac{\partial w}{\partial r}
 \end{aligned}
 \tag{17}$$

Similarly, the laminated region non-zero strain and strain gradient are, respectively, written as

$$\begin{aligned}
 \epsilon_{rr} &= \frac{\partial u_0}{\partial r} - z \frac{\partial^2 w}{\partial r^2} & \epsilon_{\theta\theta} &= \frac{u_0}{r} - z \frac{\partial^2 w}{r \partial r} \\
 \eta_{rrr} &= \frac{\partial^2 u_0}{\partial r^2} - z \frac{\partial^3 w}{\partial r^3} & \eta_{zrr} &= -\frac{\partial^2 w}{\partial r^2} & \eta_{z\theta\theta} &= -\frac{1}{r} \frac{\partial w}{\partial r} \\
 \eta_{r\theta\theta} &= -\frac{u_0}{r^2} + \frac{1}{r} \frac{\partial u_0}{\partial r} - z \frac{1}{r} \frac{\partial^2 w}{\partial r^2} + \frac{1}{r^2} z \frac{\partial w}{\partial r} \\
 \eta_{\theta\theta r} &= -\frac{u_0}{r^2} + \frac{1}{r} \frac{\partial u_0}{\partial r} - z \frac{1}{r} \frac{\partial^2 w}{\partial r^2} + \frac{1}{r^2} z \frac{\partial w}{\partial r}
 \end{aligned}
 \tag{18}$$

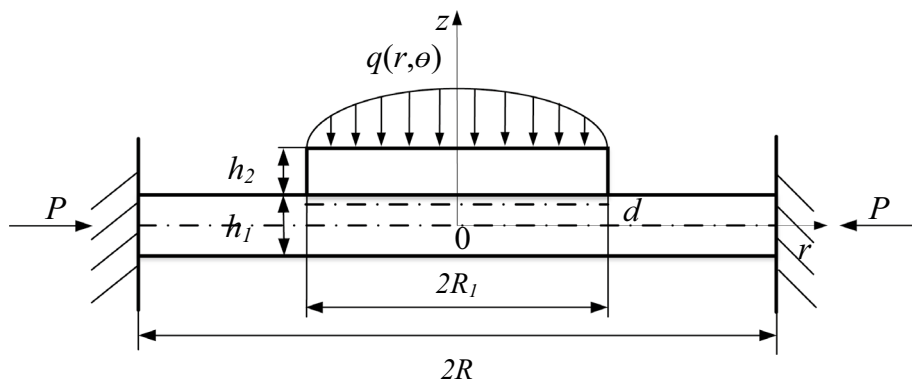
In Eq. (18), the axial displacement is $u_0 = -d \cdot \partial w / \partial r$.

Based on Eqs. (7) and (17), the non-laminated region strain energy U_1 is derived as

$$U_1 = \frac{1}{2} \int_{-\frac{1}{2}h_2}^{\frac{1}{2}h_2} \int_{R_1}^R \int_0^{2\pi} w_1 r d\theta dr dz
 \tag{19}$$

with

Fig. 1 The mechanical response of the partially covered laminated circular microplate



$$\begin{aligned}
 w_1 = & (c_{1(1)}z^2 + c_{3(1)}) \left[(w^{(2)})^2 + \frac{1}{r^2} (w^{(1)})^2 \right] \\
 & + (c_{2(1)}z^2 + c_{4(1)}) \left[w^{(2)} \frac{1}{r} w^{(1)} \right] \\
 & + c_{5(1)}z^2 (w^{(2)})^3 \\
 & + c_{6(1)}z^2 \left[\frac{1}{r^2} (w^{(2)})^2 - \frac{1}{r^3} w^{(1)} w^{(2)} + \frac{1}{r^4} (w^{(1)})^2 \right] \\
 & + c_{7(1)}z^2 \left[\frac{1}{r^2} w^{(3)} w^{(1)} - \frac{1}{r^2} w^{(3)} w^{(1)} \right]
 \end{aligned} \tag{20}$$

In Eq. (20), $w^{(i)} (i = 1, 2, 3) = dw^{(i)} / dr^i$.

Similarly, using Eqs. (7) and (18), the laminated region strain energy U_2 is derived as

$$\begin{aligned}
 U_2 = & \frac{1}{2} \int_{-\frac{1}{2}h_2}^{\frac{1}{2}h_2} \int_0^{R_1} \int_0^{2\pi} w_1 r d\theta dr dz \\
 & + \frac{1}{2} \int_{\frac{1}{2}h_2}^{h_1 + \frac{1}{2}h_2} \int_0^{R_1} \int_0^{2\pi} w_2 r d\theta dr dz
 \end{aligned} \tag{21}$$

with

$$\begin{aligned}
 w_2 = & c_{1(2)} \left[(u_0^{(1)})^2 + \frac{1}{r^2} u_0^2 \right] + c_{2(2)} u_0 \frac{1}{r} u_0^{(1)} \\
 & + c_{5(2)} (u_0^{(2)})^2 - 2c_{2(2)} z u_0^{(2)} w^{(3)} \\
 & + c_{6(2)} \left[\frac{1}{r^4} u_0^2 - \frac{1}{r^3} u_0 u_0^{(1)} + \frac{1}{r^2} (u_0^{(1)})^2 \right] \\
 & + c_{7(2)} \left[-\frac{1}{r^2} u_0 u_0^{(2)} + \frac{1}{r} u_0^{(1)} u_0^{(2)} \right] \\
 & + c_{1(2)} z \left[-2u_0^{(1)} w^{(2)} - 2\frac{1}{r^2} u_0 w^{(1)} \right] \\
 & - c_{2(2)} z \left[\frac{1}{r} u_0^{(1)} w^{(1)} + u_0 w^{(2)} \right] \\
 & + c_{6(2)} z \left[\frac{1}{r^3} u_0 w^{(2)} - \frac{1}{r^4} u_0 w^{(1)} \right. \\
 & \left. - \frac{1}{r^2} u_0^{(1)} w^{(2)} + \frac{1}{r^3} u_0^{(1)} w^{(1)} \right] \\
 & + c_{7(2)} z \left[-\frac{1}{r} u_0^{(2)} w^{(2)} + \frac{1}{r^2} u_0^{(2)} w^{(1)} \right. \\
 & \left. + \frac{1}{r^2} u_0^{(1)} w^{(3)} - \frac{1}{r} u_0^{(1)} w^{(3)} \right]
 \end{aligned} \tag{22}$$

In Eq. (22), $u_0^{(i)} (i = 1, 2) = du_0^{(i)} / dr^i$. The parameters $c_{n(i)} (n = 1, 2, \dots, 7, i = 1, 2)$ are given as

$$\begin{aligned}
 c_{1(i)} = & \frac{E_i}{2(1 - \nu_i)} & c_{2(i)} = & \frac{E_i \nu_i}{(1 - \nu_i^2)} \\
 c_{3(i)} = & \frac{1}{3} \mu_{(i)} (4l_{0(i)}^2 + 3l_{1(i)}^2 + 4l_{2(i)}^2) \\
 c_{4(i)} = & \frac{2}{3} \mu_{(i)} (4l_{1(i)}^2 + l_{2(i)}^2) \\
 c_{5(i)} = & \mu_{(i)} (2l_{0(i)}^2 + l_{1(i)}^2 + l_{2(i)}^2) \\
 c_{6(i)} = & \mu_{(i)} (2l_{0(i)}^2 + 3l_{1(i)}^2 + 6l_{2(i)}^2) \\
 c_{7(i)} = & \mu_{(i)} \left(\frac{8}{3} l_{0(i)}^2 - \frac{4}{3} l_{1(i)}^2 - l_{2(i)}^2 \right)
 \end{aligned} \tag{23}$$

The non-laminated region ($R_1 < x < R$) work W_1 is written as

$$\begin{aligned}
 W_1 = & \int_{R_1}^R \int_0^{2\pi} q w r dr d\theta \\
 & + \frac{1}{2} \int_{R_1}^R \int_0^{2\pi} P (w^{(1)})^2 r dr d\theta + [2\pi r V w]_{R_1}^R \\
 & + [2\pi r M w^{(1)}]_{R_1}^R + [2\pi r M^h w^{(2)}]_{R_1}^R
 \end{aligned} \tag{24}$$

where V is the shear force. M is the classical bending moment. P is the axial compressive force. M^h is the non-classical moment. The laminated region ($0 < x < R_1$) work W_2 is given as

$$\begin{aligned}
 W_2 = & \int_0^{R_1} \int_0^{2\pi} q w r dr d\theta + \frac{1}{2} \int_0^{R_1} \int_0^{2\pi} P (w^{(1)})^2 r dr d\theta \\
 & + [2\pi r V w]_0^{R_1} + [2\pi r M w^{(1)}]_0^{R_1} + [2\pi r M^h w^{(2)}]_0^{R_1}
 \end{aligned} \tag{25}$$

Using Eqs. (19), (24) and the variation principle, the following equations are obtained as

$$\begin{aligned}
 & 2\pi \int_{R_1}^R \left[-2c_{5(1)}I_1 \nabla^6 w + 2(c_{3(1)}h_1 + c_{1(1)}I_1) \nabla^4 w \right. \\
 & \left. + P \nabla^2 w - q \right] \delta w dr \\
 & + 2\pi r [V_1 - V] \delta w \Big|_{R_1}^R + 2\pi r [M_1 - M] \delta w^{(1)} \Big|_{R_1}^R \\
 & + 2\pi r [M_1^h - M^h] \delta w^{(2)} \Big|_{R_1}^R \\
 & = 0
 \end{aligned} \tag{26}$$

with

$$V_1 = 2c_{5(1)}I_1 \frac{\partial}{\partial r} \nabla^4 w - 2(c_{3(1)}h_1 + c_{1(1)}I_1) \frac{\partial}{\partial r} \nabla^2 w - Pw^{(1)} \tag{27}$$

$$\begin{aligned}
 M_1 = & -2c_{5(1)}I_1 \left(w^{(4)} + \frac{1}{r} w^{(3)} - \frac{3}{r^2} w^{(2)} + \frac{3}{r^3} w^{(1)} \right) - c_{7(1)}I_1 \\
 & \left(\frac{1}{r^2} w^{(2)} - \frac{1}{r^3} w^{(1)} \right) - c_{3(1)}I_1 \frac{1}{r} w^{(1)} \\
 & + c_{4(1)}h_1 \frac{1}{r} w^{(1)} + 2c_{3(1)}h_1 w^{(2)} \\
 & + 2(c_{3(1)}h_1 + c_{1(1)}I_1) \nabla^2 w
 \end{aligned} \tag{28}$$

$$M_1^h = 2c_{5(1)}I_1 w^{(3)} - c_{7(1)}I_1 \left(\frac{1}{r} w^{(2)} - \frac{1}{r^2} w^{(1)} \right) \tag{29}$$

From Eq.(26), we derive the governing equation as

$$-2c_{5(1)}I_1 \nabla^6 w + 2(c_{3(1)}h_1 + c_{1(1)}I_1) \nabla^4 w + P \nabla^2 w - q = 0 \tag{30}$$

The boundary conditions are derived as

$$\begin{aligned}
 [V_1 - V] \delta w \Big|_{R_1}^R = 0 \quad [M_1 - M] \delta w^{(1)} \Big|_{R_1}^R = 0 \\
 [M_1^h - M^h] \delta w^{(2)} \Big|_{R_1}^R = 0
 \end{aligned} \tag{31}$$

Similarly, based on Eqs. (21), (25) and the variation principle, the following equations are derived as

$$\begin{aligned}
 & 2\pi \int_0^{R_1} [-A_1 \nabla^6 w + A_2 \nabla^4 w + A_3 \nabla^6 u - A_4 \nabla^4 u + P \nabla^2 w - q] \delta w dr \\
 & + 2\pi \int_0^{R_1} \left[\frac{\partial}{\partial r} (-A_3 \nabla^4 w + A_4 \nabla^2 w + A_5 \nabla^4 u - A_6 \nabla^2 u) \right] \delta u_0 dr \\
 & + 2\pi r [V_2 - V] \delta w \Big|_0^{R_1} + 2\pi r [M_2 - M] \delta w^{(1)} \Big|_0^{R_1} \\
 & + 2\pi r [M_2^h - M^h] \delta w^{(2)} \Big|_0^{R_1} \\
 & + 2\pi r F \delta u_0 \Big|_0^{R_1} + 2\pi r F^h \delta u_0^{(1)} \Big|_0^{R_1} = 0
 \end{aligned} \tag{32}$$

where u is the primitive function of the u_0 , namely, $u_0 = \partial u / \partial r$. F is the axial force. F^h is the non-classical axial force.

with

$$\begin{aligned}
 V_2 = & A_1 \frac{\partial}{\partial r} \nabla^4 w - A_2 \frac{\partial}{\partial r} \nabla^2 w - A_3 \frac{\partial}{\partial r} \nabla^4 u \\
 & + A_4 \frac{\partial}{\partial r} \nabla^2 u - Pw^{(1)}
 \end{aligned} \tag{33}$$

$$\begin{aligned}
 M_2 = & -A_1 \left[w^{(4)} + \frac{1}{r} w^{(3)} - \frac{3}{r^2} w^{(2)} + \frac{3}{r^3} w^{(1)} \right] \\
 & - A_7 \left[\frac{1}{r^2} w^{(2)} - \frac{1}{r^3} w^{(1)} \right] \\
 & - [(2c_{1(1)} - c_{2(1)})I_1 + (2c_{1(2)} - c_{2(2)})I_1] \frac{1}{r} w^{(1)} \\
 & + [c_{4(1)}h_1 + c_{4(2)}h_2] \frac{1}{r} w^{(1)} \\
 & + 2[(2c_{1(1)} - c_{2(1)})h_1 + (2c_{1(2)} - c_{2(2)})h_2] w^{(2)} \\
 & + A_2 \nabla^4 w + A_3 \left[u_0^{(4)} + \frac{1}{r} u_0^{(2)} \right. \\
 & \left. - \frac{3}{r^2} u_0^{(1)} + \frac{1}{r^3} u_0 \right] + A_8 \left[\frac{1}{r^2} u_0^{(1)} - \frac{3}{r^3} u_0 \right] \\
 & + [(2c_{1(1)} - c_{2(1)})S_1 + (2c_{1(2)} - c_{2(2)})S_2] \frac{1}{r} u_0 \\
 & - A_4 \nabla^2 u
 \end{aligned} \tag{34}$$

$$\begin{aligned}
 M_2^h = & A_1 w^3 + A_7 \left[\frac{1}{r} w^{(2)} - \frac{1}{r^2} w^{(1)} \right] - A_3 u_0^{(2)} \\
 & - A_8 \left[\frac{1}{r} u_0^{(1)} - \frac{1}{r^2} u_0 \right]
 \end{aligned} \tag{35}$$

$$\begin{aligned}
 F = & A_3 \left[w^{(4)} + \frac{1}{r} w^{(3)} - \frac{3}{r^2} w^{(2)} + \frac{3}{r^3} w^{(1)} \right] \\
 & + A_8 \left[\frac{1}{r^2} w^{(2)} - \frac{1}{r^3} w^{(1)} \right] \\
 & + [(2c_{1(1)} - c_{2(1)})S_1 + (2c_{1(2)} - c_{2(2)})S_2] \frac{1}{r} w^{(1)} - A_4 \nabla^2 w \\
 & - [(2c_{1(1)} - c_{2(1)})h_1 + (2c_{1(2)} - c_{2(2)})h_2] \frac{1}{r} u_0 + A_6 \nabla^2 u \\
 & - A_9 \left[\frac{1}{r^2} u_0^{(1)} - \frac{1}{r^3} u_0 \right] \\
 & - A_5 \left[u_0^{(3)} + \frac{1}{r} u_0^{(2)} - \frac{3}{r^2} u_0^{(1)} + \frac{3}{r^3} u_0 \right]
 \end{aligned} \tag{36}$$

$$\begin{aligned}
 F^h = & -A_3 w^{(3)} - A_8 \left[\frac{1}{r} w^{(2)} - \frac{1}{r^2} w^{(1)} \right] \\
 & + A_5 u_0^{(2)} + A_9 \left[\frac{1}{r} u_0^{(1)} - \frac{1}{r^2} u_0 \right]
 \end{aligned} \tag{37}$$

where $S_i (i = 1, 2)$ are the static moment. $A_{n(i)} (n = 1, 2, \dots, 6, i = 1, 2)$ are material parameters and given as

$$\begin{aligned}
 A_1 &= 2(c_{5(1)}I_1 + c_{5(2)}I_2) \\
 A_2 &= 2(c_{3(1)}h_1 + c_{3(2)}h_2 + c_{1(1)}I_1 + c_{1(2)}I_2) \\
 A_3 &= 2(c_{5(1)}S_1 + c_{5(2)}S_2) \\
 A_4 &= 2(c_{1(1)}S_1 + c_{1(2)}S_2) \\
 A_5 &= 2(c_{5(1)}h_1 + c_{5(2)}h_2) \\
 A_6 &= 2(c_{1(1)}h_1 + c_{1(2)}h_2) \\
 A_7 &= c_{7(1)}I_1 + c_{7(2)}I_2 \quad A_8 = c_{7(1)}S_1 + c_{7(2)}S_2 \\
 A_9 &= c_{7(1)}h_1 + c_{7(2)}h_2
 \end{aligned}
 \tag{38}$$

From Eq. (32), we obtain the laminated region ($0 < x < R_1$) governing equations as

$$\begin{aligned}
 -A_1 \nabla^6 w + A_2 \nabla^4 w + A_3 \nabla^6 u - A_4 \nabla^4 u + P \nabla^2 w - q &= 0 \\
 \frac{\partial}{\partial r} (-A_3 \nabla^4 w + A_4 \nabla^2 w + A_5 \nabla^4 u - A_6 \nabla^2 u) &= 0
 \end{aligned}
 \tag{39}$$

The laminated region ($0 < x < R_1$) boundary conditions are derived as

$$\begin{aligned}
 [V_2 - V] \delta w \Big|_0^{R_1} &= 0 \quad [M_2 - M] \delta w^{(1)} \Big|_0^{R_1} = 0 \\
 [M_2^h - M^h] \delta w^{(2)} \Big|_0^{R_1} &= 0 \\
 F \delta u_0 \Big|_0^{R_1} = F^h \delta u_0^{(1)} \Big|_0^{R_1} &= 0
 \end{aligned}
 \tag{40}$$

The governing equation in Eqs. (30), (39) and boundary conditions in Eqs. (31), (40) of the general theory are simplified as those of the modified strain gradient elasticity theory when the length parameters satisfy $l_{3(j)} = l_{0(j)}, l_{4(j)} = l_{1(j)}, l_{2(j)} = \frac{\sqrt{2}}{2} l_{5(j)} (j = 1, 2)$. Similarly, when the length parameters satisfy $l_{0(j)} = 0, l_{1(j)} = 0, l_{2(j)} = \frac{\sqrt{2}}{2} l_{5(j)} (j = 1, 2)$, the boundary conditions and governing equation of the modified couple stress theory are also obtained from those of the general theory. In addition, when the length parameters satisfy $l_{i(j)} = 0 (i = 0, 1, 2, j = 1, 2)$, the strain gradient effects is vanished, thus the boundary conditions and governing equations of the general theory are simplified as those of classical theory.

4 On the bending of the microplate

The static bending governing equation ($R_1 < r < R$) is reduced from the Eq. (30) by ignoring the axial force P and the transverse load $q(r, \theta)$ as

$$(2(c_{3(1)}h_1 + c_{1(1)}I_1) - 2c_{5(1)}I_1 \nabla^2) \nabla^4 w_1 = 0
 \tag{41}$$

The static bending boundary conditions ($R_1 < r < R$) are reduced from the Eq. (31) by ignoring the axial force P and the transverse load $q(r, \theta)$ as

$$\begin{aligned}
 [V_{1s} - V] \delta w_1 \Big|_{R_1}^R &= 0 \quad [M_1 - M] \delta w_1^{(1)} \Big|_{R_1}^R = 0 \\
 [M_1^h - M^h] \delta w_1^{(2)} \Big|_{R_1}^R &= 0
 \end{aligned}
 \tag{42}$$

with

$$\begin{aligned}
 V_{1s} &= 2c_{5(1)}I_1 \frac{\partial}{\partial r} \nabla^4 w_1 - 2(c_{3(1)}h_1 \\
 &\quad + c_{1(1)}I_1) \frac{\partial}{\partial r} \nabla^2 w_1
 \end{aligned}
 \tag{43}$$

Similarly, the static bending governing equation ($0 < r < R_1$) is reduced from the Eqs. (39) by ignoring the axial force P as

$$\begin{aligned}
 -A_1 \nabla^6 w_2 + A_2 \nabla^4 w_2 + A_3 \nabla^6 u - A_4 \nabla^4 u - q &= 0 \\
 \frac{\partial}{\partial r} (-A_3 \nabla^4 w_2 + A_4 \nabla^2 w_2 + A_5 \nabla^4 u - A_6 \nabla^2 u) &= 0
 \end{aligned}
 \tag{44}$$

The static bending boundary conditions ($0 < r < R_1$) are reduced from the Eq. (40) by ignoring the axial force P as

$$\begin{aligned}
 [V_{2s} - V] \delta w_2 \Big|_{R_1}^R &= 0 \quad [M_1 - M] \delta w_2^{(1)} \Big|_{R_1}^R = 0 \\
 [M_1^h - M^h] \delta w_2^{(2)} \Big|_{R_1}^R &= 0
 \end{aligned}
 \tag{45}$$

with

$$\begin{aligned}
 V_{2s} &= A_1 \frac{\partial}{\partial r} \nabla^4 w_2 - A_2 \frac{\partial}{\partial r} \nabla^2 w_2 \\
 &\quad - A_3 \frac{\partial}{\partial r} \nabla^4 u + A_4 \frac{\partial}{\partial r} \nabla^2 u
 \end{aligned}
 \tag{46}$$

For the non-laminated deflection in Eq. (41), we derive the solution $w_1(r)$ as

$$w_1 = w_{s1} + w_{s2}
 \tag{47}$$

The deflection w_{s1} satisfies the following equation

$$\nabla^4 w_{s1} = 0
 \tag{48}$$

Let $r = e^t, D = d/dt$ and apply the operator method of Euler, we can obtain the following equation as

$$D^4 w_{s1} - 4D^3 w_{s1} + 4D^2 w_{s1} = 0
 \tag{49}$$

The solution of Eq. (49) is derived as

$$w_{s1} = c_1 + c_2 \ln r + c_3 r^2 + c_4 r^2 \ln r
 \tag{50}$$

The deflection w_{s2} satisfies the following equation

$$r^2 \frac{d^2 w_{s2}}{dr^2} + r \frac{dw_{s2}}{dr} - \left(\sqrt{\frac{(c_{3(1)}h_1 + c_{1(1)}I_1)}{c_{5(1)}I_1}} r \right)^2 w_{s2} = 0 \quad (51)$$

The solution of Eq. (51) is derived as

$$w_{s2} = c_5 I_0(D_1 r) + c_6 k_0(D_1 r) \quad (52)$$

with

$$D_1 = \sqrt{\frac{(c_{3(1)}h_1 + c_{1(1)}I_1)}{c_{5(1)}I_1}} \quad (53)$$

Therefore, based on Eqs. (47), (50) and (52), the deflection $w_1(r)$ ($0 < r < R_1$) is derived as

$$w_1(r) = c_1 + c_2 \ln r + c_3 r^3 + c_4 r^2 \ln r + c_5 I_0(D_1 r) + c_6 k_0(D_1 r) \quad (54)$$

Similarly, based on Eq. (44), it can be seen that the solution of Eq. (44) includes the general solution w_s and the special solution w_q . The general solution $w_s(r)$ satisfies

$$-A_1 \nabla^6 w_s + A_2 \nabla^4 w_s + A_3 \nabla^6 u - A_4 \nabla^4 u - q = 0$$

$$\frac{\partial}{\partial r} (-A_3 \nabla^4 w_s + A_4 \nabla^2 w_s + A_5 \nabla^4 u - A_6 \nabla^2 u) = 0 \quad (55)$$

Let $L_1 = -A_1 \nabla^2 + A_2$, $L_2 = -A_3 \nabla^2 - A_4$, $L_3 = -A_3 \nabla^2 + A_4$, $L_4 = A_5 \nabla^2 - A_6$ and apply the L operator method, we obtain the following equation

$$(A_3^2 - A_1 A_5) \nabla^4 w_s + (A_1 A_6 + A_2 A_5 - 2A_3 A_4) \nabla^2 w_s - A_2 A_6 + A_4^2 = c_7 + c_8 \ln r + c_9 r^2 + c_{10} r^2 \ln r \quad (56)$$

From Eq. (56), the general solution $w_s(r)$ is derived as

$$w_s(r) = a_7 + a_8 r^2 + a_9 J_0(\sqrt{s_1} r) + a_{10} J_0(\sqrt{s_2} r) + a_{11} Y_0(\sqrt{s_1} r) + a_{12} Y_0(\sqrt{s_2} r) + a_{13} \ln r + a_{14} r^2 \ln r \quad (57)$$

with

$$s_1 = \frac{s_{11} + \sqrt{s_{11}^2 - 4s_{12}s_{13}}}{2s_{12}} \quad s_2 = \frac{s_{11} - \sqrt{s_{11}^2 - 4s_{12}s_{13}}}{2s_{12}}$$

$$s_{11} = A_1 A_6 + A_5 A_2 - 2A_3 A_4 \quad s_{12} = A_3^2 + A_1 A_5$$

$$s_{13} = A_4^2 + A_2 A_6 \quad (58)$$

Considering the deflection of the middle point of the circular plate is finite, the parameters should satisfy: $a_{11} = a_{12} = a_{13} = a_{14} = 0$, thus, the general solution $w_s(r)$ is written as

$$w_s(r) = a_7 + a_8 r^2 + a_9 J_0(\sqrt{s_1} r) + a_{10} J_0(\sqrt{s_2} r) \quad (59)$$

Using Eq.(55) and the L operator method, we can also obtain

$$u(r) = a_{15} r^2 + a_{16} J_0(\sqrt{s_1} r) + a_{17} J_0(\sqrt{s_2} r) + a_{12} \quad (60)$$

Due to $u(r)$ is the primitive function of the u_0 , we obtain

$$u_0(r) = 2a_{15} r - \sqrt{s_1} a_{16} J_0(\sqrt{s_1} r) - \sqrt{s_2} a_{17} J_0(\sqrt{s_2} r) \quad (61)$$

with

$$a_{16} = \frac{A_3 s_1 + A_4}{A_5 s_1 + A_6} a_9 \quad a_{17} = \frac{A_3 s_2 + A_4}{A_5 s_2 + A_6} a_{10}. \quad (62)$$

For the plate subjected by the distributed load q , the special solution $w_q(r)$ is assumed as

$$w_q = ar^4 \quad u_q = br^4 \quad (63)$$

Based on Eqs. (44) and (63), we obtain

$$a = \frac{qA_6}{64(A_2 A_6 - A_4^2)} \quad b = \frac{qA_4}{64(A_2 A_6 - A_4^2)} \quad (64)$$

Therefore, the laminated region deflection $w_2(r)$ and axial displacement $u_0(r)$ are derived as

$$w_2(r) = a_7 + a_8 r^2 + a_9 J_0(\sqrt{s_1} r) + a_{10} J_0(\sqrt{s_2} r) + \frac{qA_6}{64(A_2 A_6 - A_4^2)}$$

$$u_0(r) = 2a_{15} r - \sqrt{s_1} a_{16} J_0(\sqrt{s_1} r) - \sqrt{s_2} a_{17} J_0(\sqrt{s_2} r) + \frac{qA_4}{64(A_2 A_6 - A_4^2)} \quad (65)$$

Using Eqs. (54) and (65), together with the boundary conditions, internal force equilibrium conditions and deformation compatibility conditions, we can figure out the unknown constants and determine the static deflection of the plate.

The deformation compatibility conditions at $r = R_1$ are given as

$$w_1(R_1) = w_2(R_1) \quad w_1^{(1)}(R_1) = w_2^{(1)}(R_1)$$

$$w_1^{(2)}(R_1) = w_2^{(2)}(R_1) \quad u_0(R_1) = 0 \quad (66)$$

The internal shear forces at $r = R_1$ should satisfy

$$\left[2c_{5(1)} I_1 \frac{\partial}{\partial r} \nabla^4 w_1 - 2(c_{3(1)} h_1 + c_{1(1)} I_1) \frac{\partial}{\partial r} \nabla^2 w_1 \right]_{r=R_1}$$

$$= \left[A_1 \frac{\partial}{\partial r} \nabla^4 w_2 - A_2 \frac{\partial}{\partial r} \nabla^2 w_2 - A_3 \frac{\partial}{\partial r} \nabla^4 u + A_4 \frac{\partial}{\partial r} \nabla^2 u \right]_{r=R_1} \quad (67)$$

The internal moments at $r = R_1$ should satisfy

$$\begin{aligned}
 & \left[-2c_{5(1)}I_1(w_1^{(4)} + \frac{1}{r}w_1^{(3)} - \frac{3}{r^2}w_1^{(2)} + \frac{3}{r^3}w_1^{(1)}) \right. \\
 & \quad - c_{7(1)}I_1\left(\frac{1}{r^2}w_1^{(2)} - \frac{1}{r^3}w_1^{(1)}\right) - c_{3(1)}I_1\frac{1}{r}w_1^{(1)} \\
 & \quad + c_{4(1)}h_1\frac{1}{r}w_1^{(1)} + 2c_{3(1)}h_1w_1^{(2)} \\
 & \quad \left. + 2(c_{3(1)}h_1) + c_{1(1)}I_1\right]\nabla^2w_1\Big|_{r=R_1} \\
 & = \left[-A_1\left(w_2^{(4)} + \frac{1}{r}w_2^{(3)} - \frac{3}{r^2}w_2^{(2)} + \frac{3}{r^3}w_2^{(1)}\right) \right. \\
 & \quad - A_7\left(\frac{1}{r^2}w_2^{(2)} - \frac{1}{r^3}w_2^{(1)}\right) \\
 & \quad - ((2c_{1(1)} - c_{2(1)})I_1 + (2c_{1(2)} - c_{2(2)})I_1)\frac{1}{r}w_2^{(1)} \\
 & \quad + (c_{4(1)}h_1 + c_{4(2)}h_2)\frac{1}{r}w_2^{(1)} + A_2\nabla^4w_2 - A_4\nabla^2u \\
 & \quad + 2((2c_{1(1)} - c_{2(1)})h_1 + (2c_{1(2)} - c_{2(2)})h_2)w_2^{(2)} \\
 & \quad + A_3\left(u_0^{(4)} + \frac{1}{r}u_0^{(2)} - \frac{3}{r^2}u_0^{(1)} + \frac{1}{r^3}u_0\right) \\
 & \quad + A_8\left(\frac{1}{r^2}u_0^{(1)} - \frac{3}{r^3}u_0\right) + ((2c_{1(1)} - c_{2(1)})S_1 + (2c_{1(2)} \\
 & \quad - c_{2(2)})S_2)\frac{1}{r}u_0\Big|_{r=R_1} \tag{68}
 \end{aligned}$$

The internal higher-order moments at $r = R_1$ should satisfy

$$\begin{aligned}
 & \left[2c_{5(1)}I_1w_1^{(3)} - c_{7(1)}I_1\left(\frac{1}{r}w_1^{(2)} - \frac{1}{r^2}w_1^{(1)}\right) \right]_{r=R_1} \\
 & = \left[A_1w_2^3 + A_7\left(\frac{1}{r}w_2^{(2)} - \frac{1}{r^2}w_2^{(1)}\right) - A_3u_0^{(2)} \right. \\
 & \quad \left. - A_8\left(\frac{1}{r}u_0^{(1)} - \frac{1}{r^2}u_0\right) \right]_{r=R_1} \tag{69}
 \end{aligned}$$

The internal axial forces at $r = R_1$ should satisfy

$$\begin{aligned}
 & \left[A_3(w_2^{(4)} + \frac{1}{r}w_2^{(3)} - \frac{3}{r^2}w_2^{(2)} + \frac{3}{r^3}w_2^{(1)}) + A_8\left(\frac{1}{r^2}w_2^{(2)} - \frac{1}{r^3}w_2^{(1)}\right) \right. \\
 & \quad + ((2c_{1(1)} - c_{2(1)})S_1 + (2c_{1(2)} - c_{2(2)})S_2)\frac{1}{r}w_2^{(1)} - A_4\nabla^2w_2 \\
 & \quad - ((2c_{1(1)} - c_{2(1)})h_1 + (2c_{1(2)} - c_{2(2)})h_2)\frac{1}{r}u_0 + A_6\nabla^2u \\
 & \quad \left. - A_9\left(\frac{1}{r^2}u_0^{(1)} - \frac{1}{r^3}u_0\right) - A_5\left(u_0^{(3)} + \frac{1}{r}u_0^{(2)} - \frac{3}{r^2}u_0^{(1)} + \frac{3}{r^3}u_0\right) \right]_{r=R_1} = 0 \tag{70}
 \end{aligned}$$

The internal higher-order axial forces at $r = R_1$ should satisfy

$$\begin{aligned}
 & \left[-A_3w_2^{(3)} - A_8\left(\frac{1}{r}w_2^{(2)} - \frac{1}{r^2}w_2^{(1)}\right) + A_5u_0^{(2)} \right. \\
 & \quad \left. + A_9\left(\frac{1}{r}u_0^{(1)} - \frac{1}{r^2}u_0\right) \right]_{r=R_1} = 0 \tag{71}
 \end{aligned}$$

For the simply supported plate, we give the boundary conditions as

$$w_1(R) = 0 \quad M_1(R) = 0 \quad M_1^{(h)}(R) = 0 \tag{72}$$

For the clamped-clamped plate, we give the boundary conditions as

$$w_1(R) = 0 \quad w_1^{(1)}(R) = 0 \quad w_1^{(2)}(R) = 0 \tag{73}$$

Using Eqs. (54), (65)–(72) or (73), we obtain the following equation

$$[M(P)]\{a\} = \{D\} \tag{74}$$

The matrix $[M(P)]$ and vector D are respectively given in the “Appendix A”. Solving Eq. (74), we can figure out the unknown constants and thus determine the static deflection of the simply supported microplate. The static deflection of the clamped-clamped microplate can also be determined in the similar way.

4.1 Numerical results

The size-dependent bending response of the microplate is studied. The material parameters of lower silicon elastic layer are $E_{(1)} = 1530$ Gpa. $\nu_{(1)} = 0.33$. The geometric parameters are $h_1 = 1 \mu\text{m}$. $R = 10h_1$. The material parameters of upper elastic layer are $E_{(2)} = 0.5E_{(1)}$. $\nu_{(2)} = 0.5\nu_{(1)}$. We define T_R as the thickness ratio, $T_R = h_2/h_1$. L_R is defined as the radius ratio, $L_R = R_1/R$. In addition, the length parameters satisfy: $l_{i(1)} = l$, $l_{i(2)} = 0.5l$ ($i = 0, 1, 2$), $l = 0.428 \mu\text{m}$ [70].

The calibration of the bending model with different boundary conditions is shown in Fig. 2. It can be seen that when the thickness ratio and length ratio satisfy $T_R = 0, L_R = 1$, the deflection of the present model with simply supported boundary conditions is the same as that of the monolayer microplate model in the Ref. [71] without the material graded parameter. When the thickness ratio and length ratio satisfy $T_R = 0.2, L_R = 1$, the present model with simply supported boundary conditions will reduce to the bilayer microplate model in the Ref. [72] without the surface effects. The degradation relations among the present model with clamped-clamped boundary conditions and the model in the Ref. [72] and Ref. [73] are also shown in Fig. 2. Thus, the effectiveness of the present model is revealed.

The maximum deflections of the partially covered laminated microplate predicted by the conventional model in Refs. [6] and [74] are respectively given in the Table 2. It can be seen that the present model can respectively reduce to the conventional model in Refs. [6] and [74] when the thickness is much larger than the material length scale parameter. The results imply that the effects from strain gradients can be ignored at this dimension. It can be also seen that the present model predicts smaller deflection than that of the conventional model in Refs. [6] and [74] when the thickness is the same as the material length scale parameter. The results imply that the effects from strain gradients should be

considered in this dimension. The limitation of the conventional model is thus revealed.

The comparison of the deflection of the clamped-clamped partially covered laminated microplate based on the present model, the experiment results in the Ref. [6] and numerical methods in the Ref. [47] is respectively shown in the Fig. 3. It can be seen that when the thickness ratio is $T_R = 0.4$, length ratio is $L_R = 0.87$, the deflection of the present model without strain gradients fits well with the experiment results in the Ref. [6]. In addition, when the thickness ratio is $T_R = 0$, length ratio is $L_R = 1$, the deflection of the present model is almost the same as that of the model without the nonlinear effects in the Ref. [47] using the differential quadrature method (DQM).

The comparison of bending response of the microplate predicted by different strain gradient models is shown in Fig. 4. It can be seen that the deflection of strain gradient model including different strain gradients is different. Compared with the reduced theories, the deflection of the general theory is much smaller. The general theory contains all strain gradients and thus predicts smaller deflection. In addition, the modified couple stress theory with the influence only from the rotation gradients predicts larger deflection. The bending rigidity of the beam of the general theory is maximum while the bending rigidity corresponding to the reduced theories is relatively smaller. The similar conclusion can also be obtained for the axial displacement.

The size-dependent bending response of the microplate is given in Fig. 5. It can be seen that the deflection decreases gradually along the radius direction from $\xi=0$ to $\xi = 1$. In addition, the variation of the deflection depends on the dimensionless thickness ξ . The deflection gradually increases with the increase of the dimensionless thickness ξ . The conventional model is unable to capture the size

Table 2 The maximum deflection of the partially covered microplate predicted by the present model and the conventional model

h/l	Clamped-Clamped microplate		Simply supported microplate	
	Present model (μm)	Ref. [6] (μm)	Present model (μm)	Ref. [74] (μm)
1	0.0235	0.9077	15.7388	399.9809
5	0.3594	0.9077	193.6944	399.9809
10	0.6563	0.9077	299.6364	399.9809
15	0.7786	0.9077	335.4767	399.9809
20	0.8343	0.9077	352.1831	399.9809
25	0.8635	0.9077	362.1958	399.9809
30	0.8805	0.9077	369.3037	399.9809
35	0.8914	0.9077	374.9456	399.9809
40	0.8987	0.9077	379.7618	399.9809

dependency of the deflection. Compared with the conventional theory, when the dimensionless thickness ξ is small, the deflection of the general theory is much smaller. As the dimensionless thickness ξ increases, the deflection of the general theory increases and closes to the conventional theory. Conventional theory underestimates the size effects.

The size effects of the axial displacement is shown in Fig. 6. It can be seen that the axial displacement increases gradually along the radius direction from $\xi = 0$ to $\xi = 1$. In addition, the variation of the axial displacement is dependent on the dimensionless thickness ξ . As the dimensionless thickness ξ increases, the axial displacement gradually increases. Classical theory is unable to predict the size effects of the axial displacement correctly. Compared with the general theory, when the dimensionless thickness is

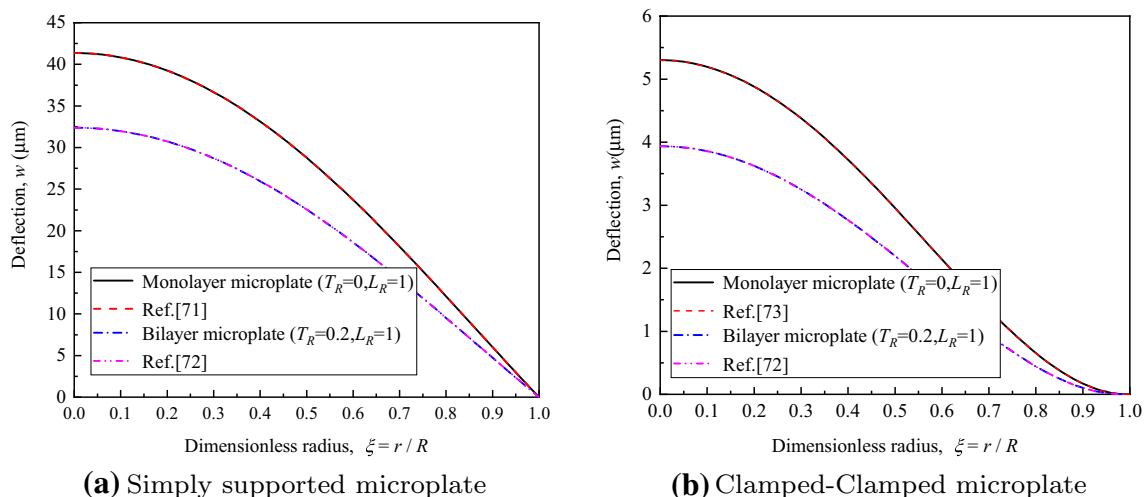


Fig. 2 Calibration of the bending model

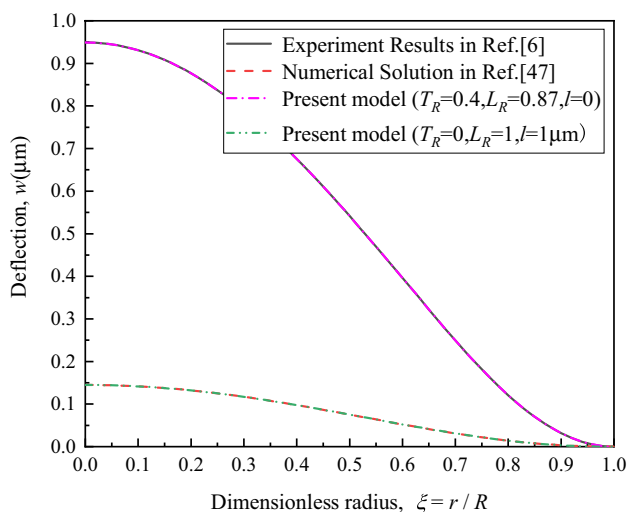


Fig. 3 The comparison of the deflection of the microplate based on different methods

$\xi = 1$, the axial displacement of the classical theory is much smaller. When the dimensionless thickness is $\xi = 50$, the axial displacement of the general theory and the classical theory is almost the same. The general theory can reflect the size dependency behaviour of the axial displacement more suitably.

The effects of the thickness and radius of laminated region on the bending response are shown in Fig. 7. The bending performance is influenced by the laminated region parameters. When the radius of the upper layer is fixed, as the increase of the thickness of the upper layer, the deflection decreases gradually. The increase of the thickness of the upper layer makes the bending rigidity increase, the beam stiffer and harder to deformation, therefore the deflection becomes relatively smaller.

When the upper layer thickness is fixed, the increase of the radius of the upper layer makes the uniformly distributed load and the stiffness increase gradually at the same time. Therefore, the influence of the radius of the upper layer on the bending deflection is dependent on the contributions of the bending stiffness, the boundary conditions and the external load. For the simply supported microplate, the increase of the radius of the upper layer makes the deflection increase gradually, which indicates that the effects of the uniformly distributed load are predominate. Therefore, for the smart microcomponents based on the bending response of the simply supported microplate, to achieve the maximum bending deflection, the radius of the upper layer should be the same as that of the lower layer.

For the clamped-clamped microplate, as the radius of the upper layer increases, the deflection gradually increases and subsequently decreases. For a certain thickness and radius of the upper layer, the deflection can obtain the maximum value.

When the thickness ratio is 1 and the radius ratio is 0.82, the deflection of the microplate is maximum.

5 On the buckling of the microplate

The buckling governing equation ($R_1 < r < R$) is obtained from the Eq.(30) by ignoring the uniformly distributed load q as

$$-2c_{5(1)}I_1 \nabla^6 w_1 + 2(c_{3(1)}h_1 + c_{1(1)}I_1) \nabla^4 w_1 + P \nabla^2 w_1 = 0 \tag{75}$$

The buckling boundary conditions ($R_1 < r < R$) are already given in the Eq. (31)

Similarly, by ignoring the uniformly distributed load q , the buckling governing equation ($0 < r < R_1$) is obtained from the Eqs. (39) as

$$\nabla^2 [(-A_1 \nabla^4 + A_2 \nabla^4 + P)w_2 + (A_3 \nabla^4 - A_4 \nabla^2)u] = 0$$

$$\frac{\partial}{\partial r} \nabla^2 [(-A_3 \nabla^2 + A_4)w_2 + (A_5 \nabla^2 u - A_6)u] = 0 \tag{76}$$

The buckling boundary conditions ($0 < r < R_1$) are already shown in the Eq.(40).

The solution $w_1(r)$ of Eq. (75) is written as

$$w_1 = w_{s1} + w_{s2} \tag{77}$$

The deflection w_{s1} satisfies the following equation

$$\nabla^4 w_{s1} = 0 \tag{78}$$

The solution of Eq. (78) is derived as

$$w_{s1} = c_1 + c_2 \ln r \tag{79}$$

The deflection w_{s2} satisfies the following equation

$$(\nabla^2 - s_1)(\nabla^2 - s_2)w_{s2} = 0 \tag{80}$$

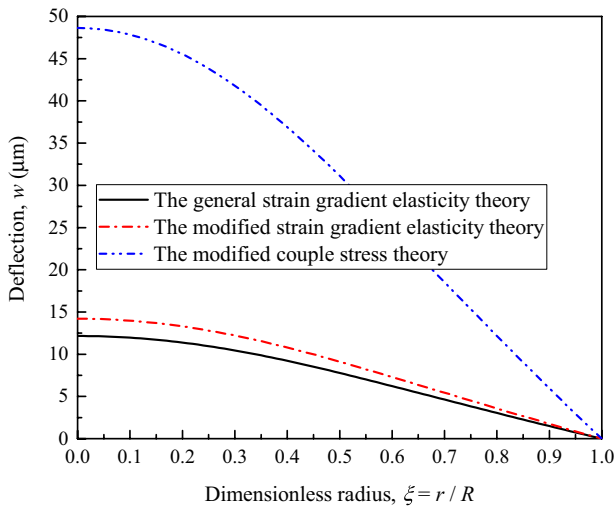
with

$$s_1 = \frac{B + \sqrt{B^2 + 4PA}}{2A} \quad s_2 = \frac{B - \sqrt{B^2 + 4PA}}{2A} \tag{81}$$

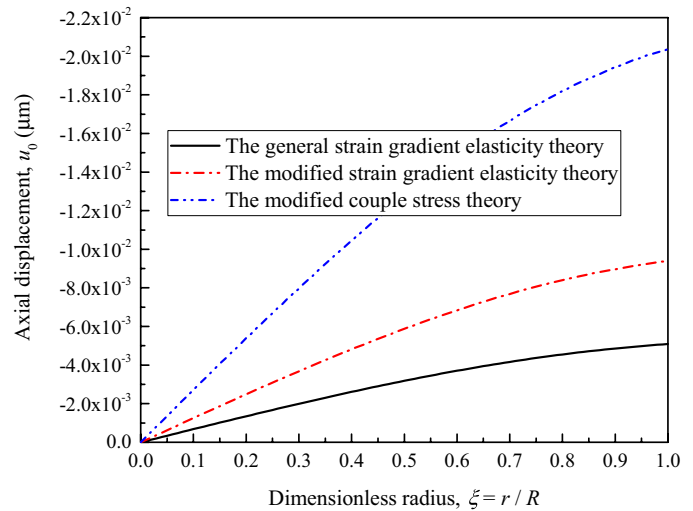
where $A = 2c_{5(1)}I_1$ and $B = 2(c_{3(1)}h_1 + c_{1(1)}I_1)$. The solution of Eq. (80) is derived as

$$w_{s2} = c_3 I_0(\sqrt{s_1}r) + c_4 K_0(\sqrt{s_1}r) + c_5 I_0(\sqrt{s_2}r) + c_6 K_0(\sqrt{s_2}r) \tag{82}$$

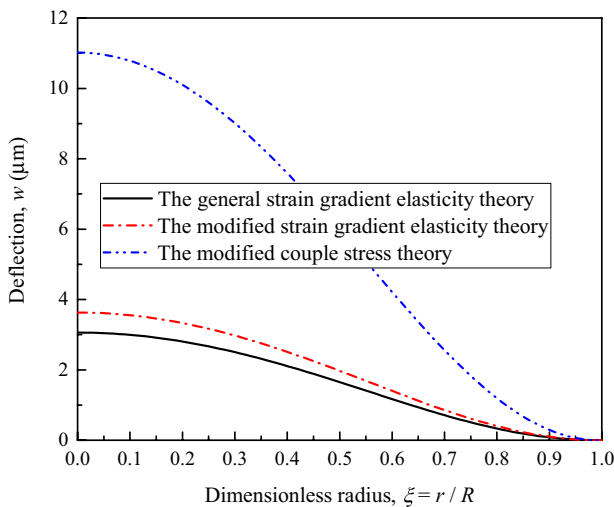
Therefore, using Eqs. (79) and (82), the non-laminated region deflection $w_1(r)$ is written as



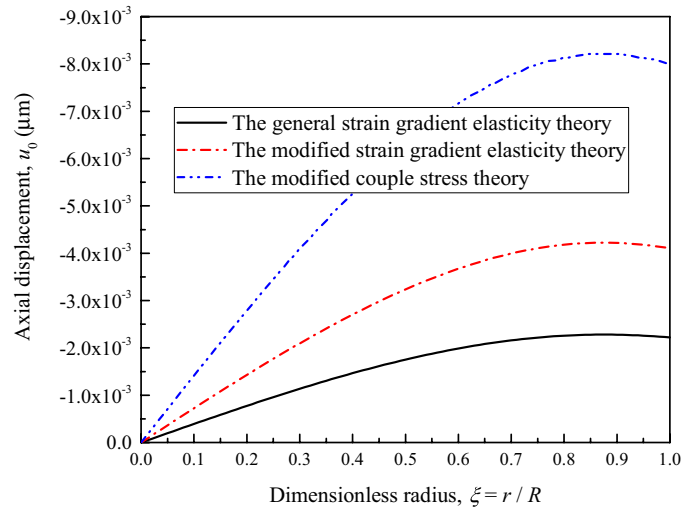
(a) Simply supported microplate



(b) Simply supported microplate



(c) Clamped-Clamped microplate



(d) Clamped-Clamped microplate

Fig. 4 Deflection and axial displacement of the microplate

$$w_1 = c_1 + c_2 \ln r + c_3 I_0(\sqrt{s_1} r) + c_4 K_0(\sqrt{s_1} r) + c_5 I_0(\sqrt{s_2} r) + c_6 K_0(\sqrt{s_2} r) \tag{83}$$

The solution $w_2(r)$ of Eq.(76) is written as

$$\begin{aligned} (-A_1 \nabla^4 + A_2 \nabla^4 + P)w_2 + (A_3 \nabla^4 - A_4 \nabla^2)u &= c_7 + c_8 \ln r \\ (-A_3 \nabla^2 + A_4)w_2 + (A_5 \nabla^2 u - A_6)u &= c_9 + c_{10} \ln r + c_{11} r^2 \end{aligned} \tag{84}$$

Let $L_1 = -A_1 \nabla^4 + A_2 \nabla^4 + P$, $L_2 = A_3 \nabla^4 - A_4 \nabla^2$, $L_3 = -A_3 \nabla^2 + A_4$, $L_4 = A_5 \nabla^2 u - A_6$ and apply the L operator method, we obtain the following equation

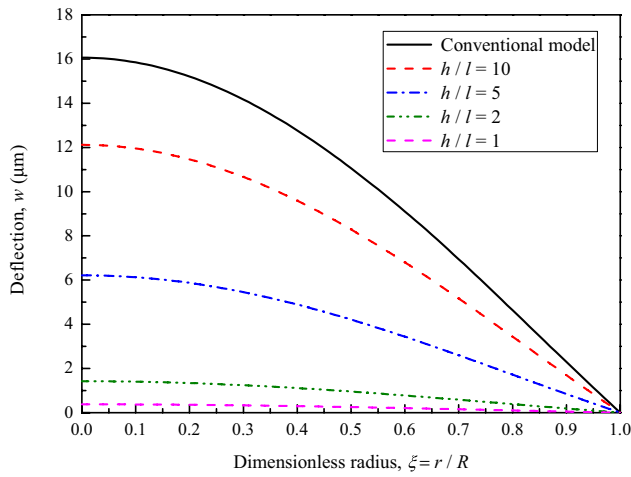
$$a \nabla^6 w_2 + b \nabla^4 w_2 + c \nabla^2 w_2 = PA_6 + D_1 + D_2 \ln r \tag{85}$$

with

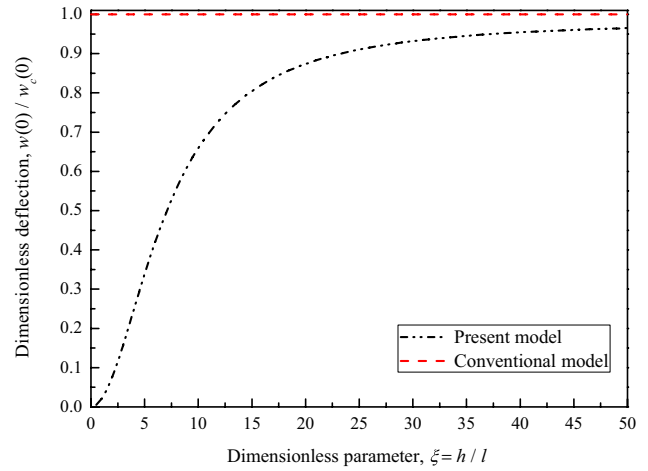
$$\begin{aligned} a &= A_3^2 - A_1 A_5 & b &= A_1 A_6 + A_5 A_2 - 2A_3 A_4 \\ c &= PA_5 + A_6 A_2 - A_4^2 \end{aligned} \tag{86}$$

It can be seen that the solution of Eq. (85) includes the general solution $w_s(r)$ and the special solution $w_q(r)$. The general solution $w_s(r)$ satisfies

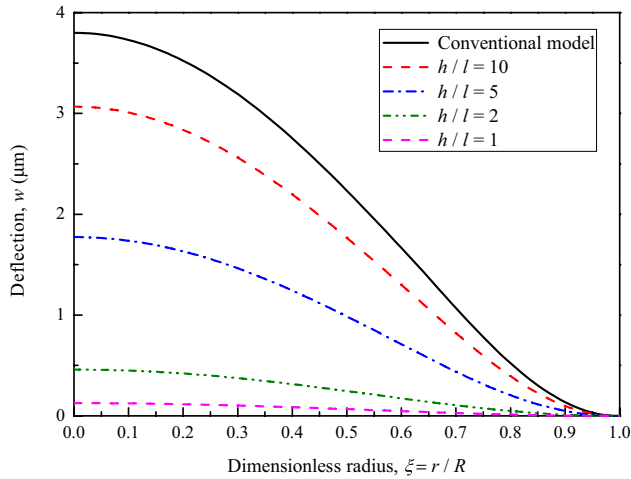
$$\nabla^2 (\nabla^2 + s_3) (\nabla^2 + s_4) w_s = 0 \tag{87}$$



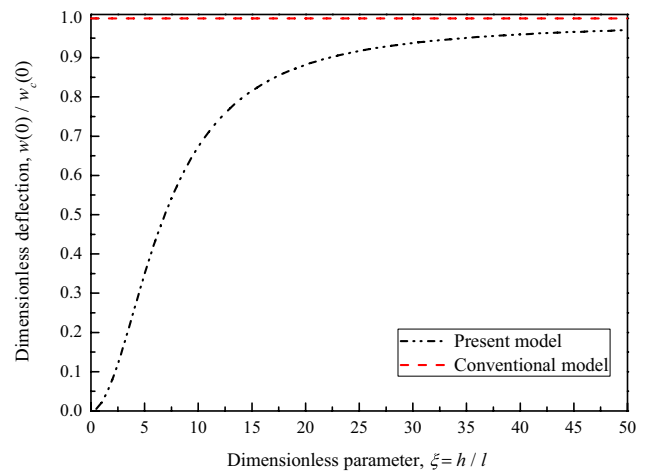
(a) Simply supported microplate



(b) Simply supported microplate



(c) Clamped-Clamped microplate



(d) Clamped-Clamped microplate

Fig. 5 Size effects of the deflection

with

$$s_3 = \frac{b + \sqrt{b^2 - 4ac}}{2a} \quad s_4 = \frac{b - \sqrt{b^2 - 4ac}}{2a} \quad (88)$$

The general solution $w_s(r)$ is derived as

$$w_s = c_{12} + c_{13} \ln r + c_{14} J_0(\sqrt{s_3}r) + c_{15} Y_0(\sqrt{s_3}r) + c_{16} J_0(\sqrt{s_4}r) + c_{17} Y_0(\sqrt{s_4}r) \quad (89)$$

The special solution $w_q(r)$ can also be derived as

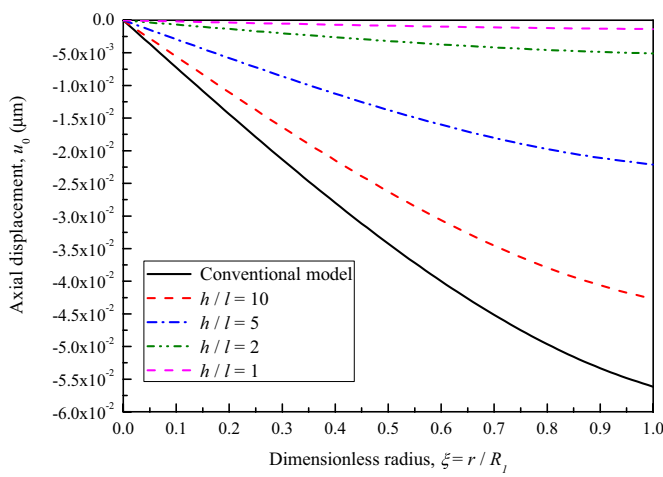
$$w_q = \frac{PA_6}{4c} r^2 + c_{18} r^2 + c_{19} r^2 \ln r \quad (90)$$

Therefore, using Eqs. (89) and (90), the laminated region deflection $w_2(r)$ is written as

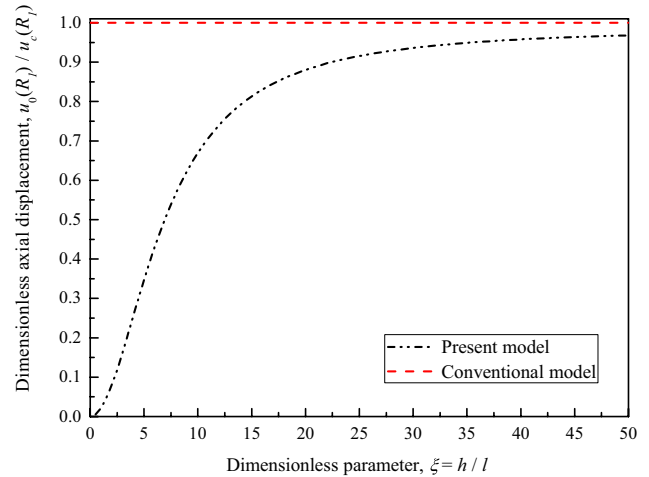
$$w_2 = c_{12} + c_{13} \ln r + c_{14} J_0(\sqrt{s_3}r) + c_{15} Y_0(\sqrt{s_3}r) + c_{16} J_0(\sqrt{s_4}r) + \frac{PA_6}{4c} r^2 + c_{18} r^2 + c_{19} r^2 \ln r \quad (91)$$

Because the laminated region deflection of the middle point of the plate is finite, thus $c_{13} = c_{15} = c_{17} = c_{19} = 0$. The deflection $w_2(r)$ is written as

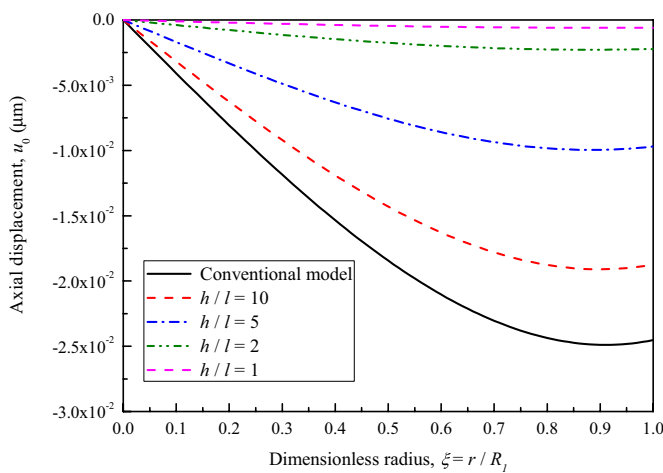
$$w_2 = c_{12} + c_{14} J_0(\sqrt{s_3}r) + c_{16} J_0(\sqrt{s_4}r) + \frac{PA_6}{4c} r^2 + c_{18} r^2 \quad (92)$$



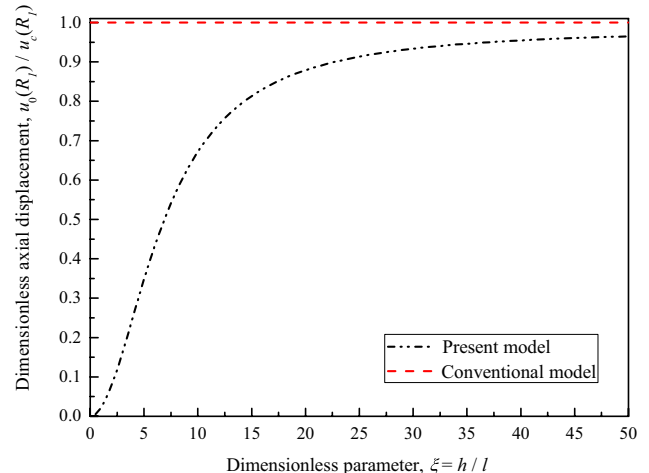
(a) Simply supported microplate



(b) Simply supported microplate



(c) Clamped-Clamped microplate



(d) Clamped-Clamped microplate

Fig. 6 Size effects of the axial displacement

Similarly, based on Eq. (84), we obtain

$$u(r) = c_{19} + mc_{14}J_0(\sqrt{s_3}r) + nc_{16}J_0(\sqrt{s_4}r) + \frac{PA_6}{4c}r^2 + c_{20}r^2 \tag{93}$$

Due to $u(r)$ is the primitive function of $u_0(r)$, thus the axial displacement $u_0(r)$ is derived as

$$u_0(r) = -m\sqrt{s_3}c_{14}J_0(\sqrt{s_3}r) - n\sqrt{s_4}c_{16}J_0(\sqrt{s_4}r) + \frac{PA_6}{2c}r + c_{21}r \tag{94}$$

with

$$m = \frac{A_3s_1 + A_4}{A_5s_1 + A_6} \quad n = \frac{A_3s_2 + A_4}{A_5s_2 + A_6} \tag{95}$$

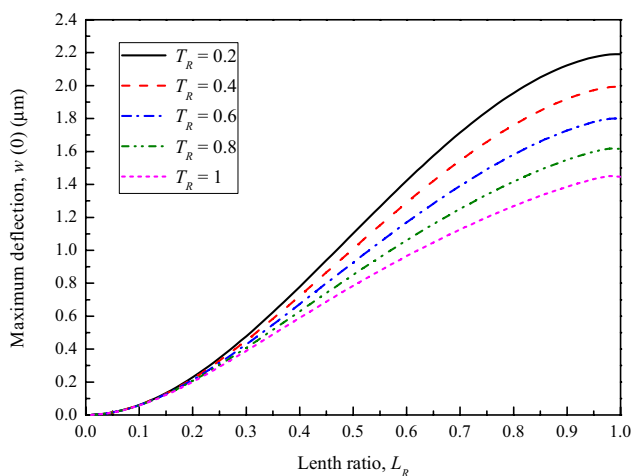
Thus, the laminated region deflection $w_2(r)$ and axial displacement $u_0(r)$ are respectively written as

$$w_2(r) = c_{12} + c_{14}J_0(\sqrt{s_3}r) + c_{16}J_0(\sqrt{s_4}r) + \frac{PA_6}{4c}r^2 + c_{18}r^2 \tag{96}$$

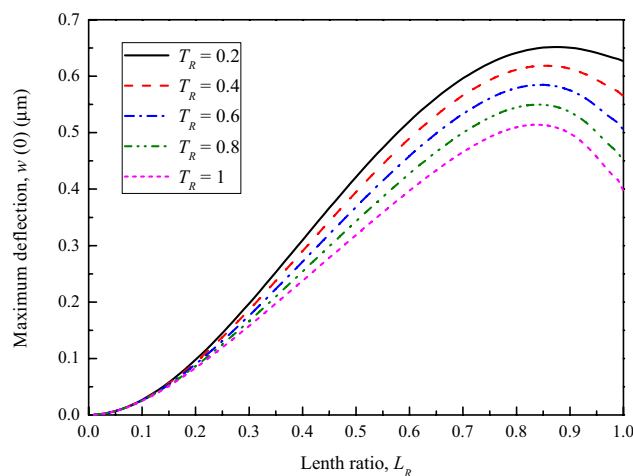
$$u_0(r) = -m\sqrt{s_3}c_{14}J_0(\sqrt{s_3}r) - n\sqrt{s_4}c_{16}J_0(\sqrt{s_4}r) + \frac{PA_6}{2c}r + c_{21}r$$

Based on Eqs. (83) and (96), using the boundary conditions, deformation compatibility conditions and internal force equilibrium conditions, we can figure out the buckling load of the plate.

The deformation compatibility conditions, the internal moments equilibrium conditions, the internal higher-order



(a) Simply supported microplate



(b) Clamped-Clamped microplate

Fig. 7 Influence of the geometric parameters of the laminated area on the deflection

moment equilibrium conditions, the internal axial force equilibrium conditions and the internal non-classical axial force equilibrium conditions are same as those of the bending problem, see Eqs. (66), (68)–(71). However, the internal shear force equilibrium conditions at $r = R_1$ of the buckling problem are different from that in the bending problem, and written as

$$\begin{aligned} & \left[2c_{5(1)}I_1 \frac{\partial}{\partial r} \nabla^4 w_1 - 2(c_{3(1)}h_1 + c_{1(1)}I_1) \frac{\partial}{\partial r} \nabla^2 w - Pw_1^{(1)} \right]_{r=R_1} \\ & = \left[A_1 \frac{\partial}{\partial r} \nabla^4 w_2 - A_2 \frac{\partial}{\partial r} \nabla^2 w_2 - A_3 \frac{\partial}{\partial r} \nabla^4 u + A_4 \frac{\partial}{\partial r} \nabla^2 u - Pw_2^{(1)} \right]_{r=R_1} \end{aligned} \tag{97}$$

The boundary conditions are already given in Eqs. (72) and (73).

Using Eqs. (83), (96) and (66) (68)–(72), (97), the following equation is obtained as

$$[M_2(P)]\{C\} = \{0\} \tag{98}$$

For a non-trivial solution, the matrix $[M_2(P)]$ should satisfy

$$|M_2(P)| = 0 \tag{99}$$

By solving Eq. (99), the buckling load is obtained. Similarly, the buckling load of the microplate under other boundary conditions can also be derived.

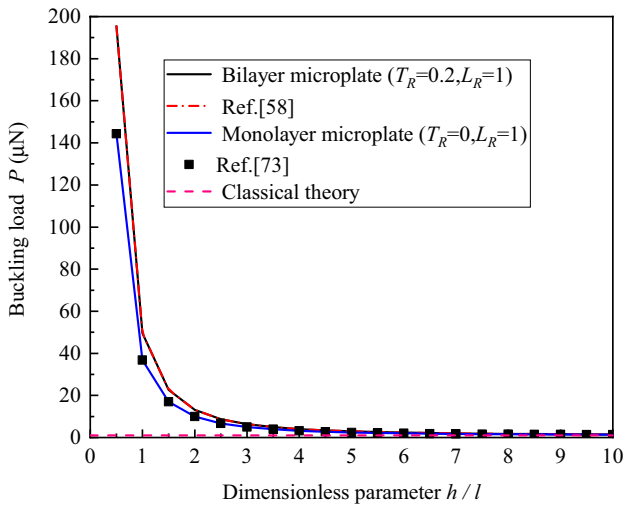
5.1 Numerical results

The calibration of the bucking model is shown in the Fig. 8. The dimensionless buckling load P_{non} is defined as $P_{non} = P/P_c$. P_c and P are the buckling load of the conventional model and the strain gradient model, respectively. It can be seen that if the thickness ratio and length ratio

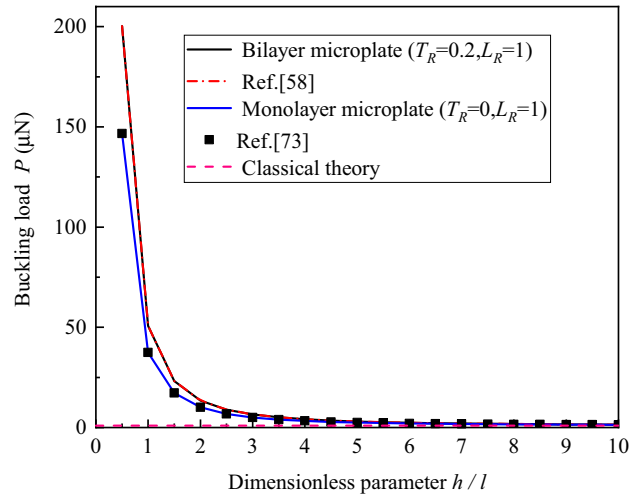
satisfy $T_R = 0, L_R = 1$, the present model with simply supported boundary conditions will reduce to the monolayer microplate model in the Ref. [73]. If the thickness ratio and length ratio satisfy $T_R = 0.2, L_R = 1$, the buckling load of present model with simply supported boundary conditions and the bilayer microplate model in the Ref. [58] without the material graded parameter are the same. The degradation relations among the present model with clamped-clamped boundary conditions and the model in the Ref. [58] and Ref. [73] are also given in Fig. 8. Thus, the validation of the present model is indicated.

The size-dependent buckling response is given in Fig. 9. It can be seen that the dimensionless buckling load is determined by the parameter h/l , gradually decreases with the increase of the parameter h/l and thus shows size dependency obviously. When the parameter satisfies $h/l = 1$, the buckling load predicted by the general theory is about 50 times of that predicted by the classical theory. This indicates that at this dimensionless thickness, the effects of strain gradient are obvious and should be considered. The classical model without the strain gradients is unable to describe the size dependency of the buckling load, and thus predict smaller buckling load. In addition, when the parameter is $h/l = 10$, the buckling load predicted by the general theory is almost the same as that of the classical theory. This indicates that at this dimensionless thickness, the effects of strain gradient is weak. In addition, compared with the general theory, the buckling load of the reduced theories is relative smaller. The reduced theories contain part of the strain gradients, therefore, underestimate the buckling response.

The influences of the geometric parameters of the laminated region on the buckling response are shown in Fig. 10. It can be seen that when the thickness or radius of the upper



(a) Simply supported microplate



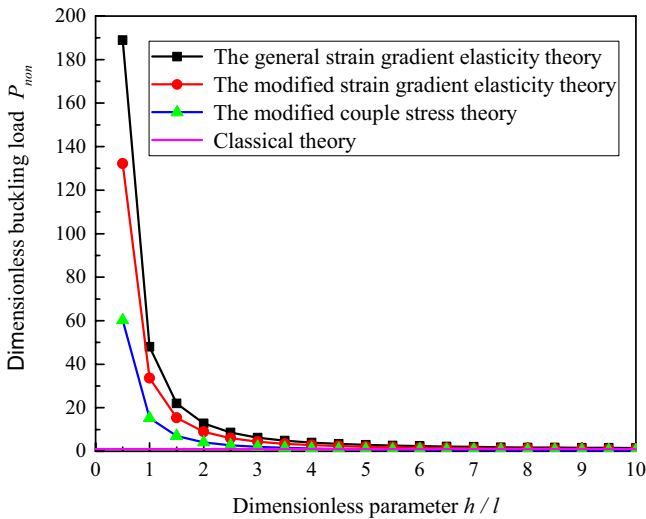
(b) Clamped-Clamped microplate

Fig. 8 Calibration of the bucking model

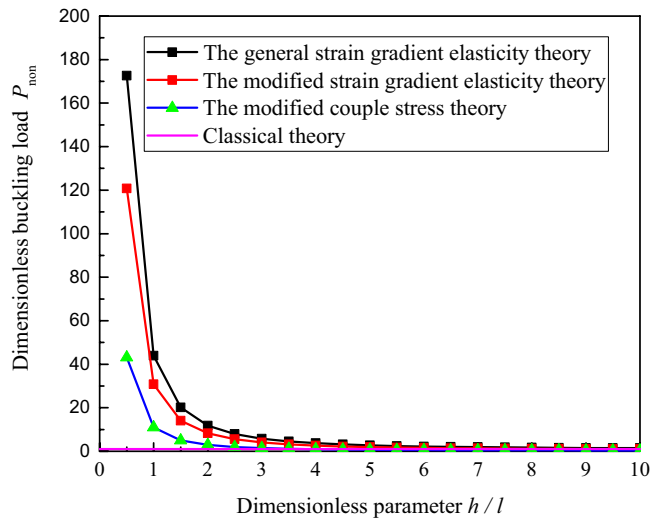
layer increases, the buckling load gradually increases. The increase of the geometric parameters of the laminated region makes the increase of the rigidity and thus enhances the ability of the micoplate to resist the deformation. When the radius ratio is taken as $l_R = 0$, the size-dependent partially covered laminated micoplate mode reduces to the monolayer micoplate model. At this radius ratio, the buckling load is minimum and the micoplate is easy to deformation. When the radius ratio is taken as $l_R = 1$, the size-dependent partially covered laminated micoplate mode reduces to the bilayer micoplate model. At this radius ratio, the buckling

load is maximum and the micoplate is hard to deformation. In addition, the buckling load of the micoplate under various boundary conditions is different. The buckling load of the clamped-clamped micoplate is obviously larger than that of the simply supported micoplate.

The influences of the length parameters on the buckling response are shown in Fig. 11. It can be seen that compared with strain gradient buckling model, classical buckling model predicts a smaller buckling load. Classical buckling model without the length parameters is unable to describe the strain gradient effects and thus underestimates the size

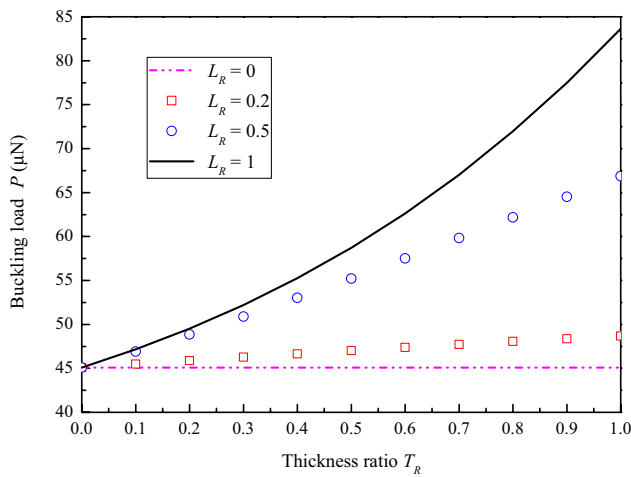


(a) Simply supported microplate

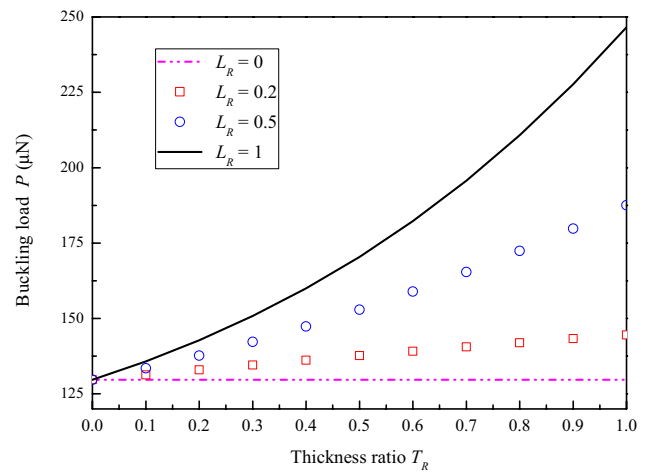


(b) Clamped-Clamped microplate

Fig. 9 Size effects of the buckling response



(a) Simply supported microplate



(b) Clamped-Clamped microplate

Fig. 10 Influences of the dimension of the laminated region on the buckling load

effects. In addition, it can also be seen that the ability of the size-dependent models including different length parameters to describe the buckling response is different. Different length parameters stand for the influences from different strain gradients. l_0 is corresponding to the dilatation gradients, l_1 is corresponding to the stretch gradients, and l_2 is corresponding to the rotation gradients. The buckling load of the size-dependent model including the length parameter l_0 is maximum. However, the buckling load of the size-dependent model with the length parameter l_1 is minimum. Namely, the stretch gradients have little contribution to the buckling deformation compared with the dilatation gradients and rotation gradients.

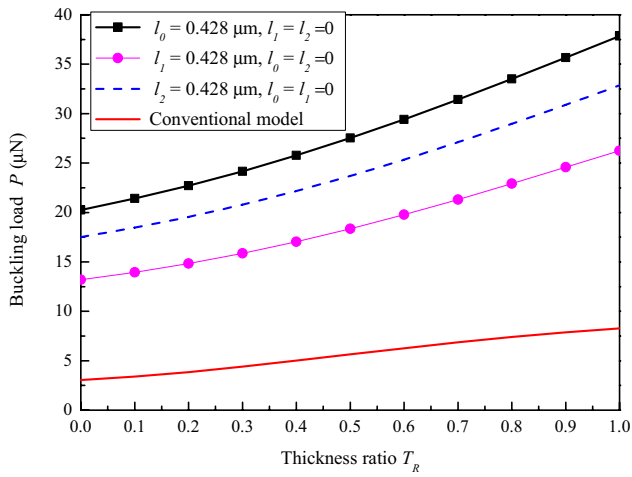
6 Conclusions

In this paper, the relations between the general theory and other strain gradient theories are identified, and the degradation relation are clarified. Subsequently, the bending and buckling analysis of the partially covered laminated microplate with strain gradient effects are performed. The expression of the axial displacement, bending deflection and buckling load of the microplate is derived. The size dependency of the axial displacement, deflection and buckling load are studied. The influences from material parameters and the laminated region geometric parameters on the deflection and buckling load are studied.

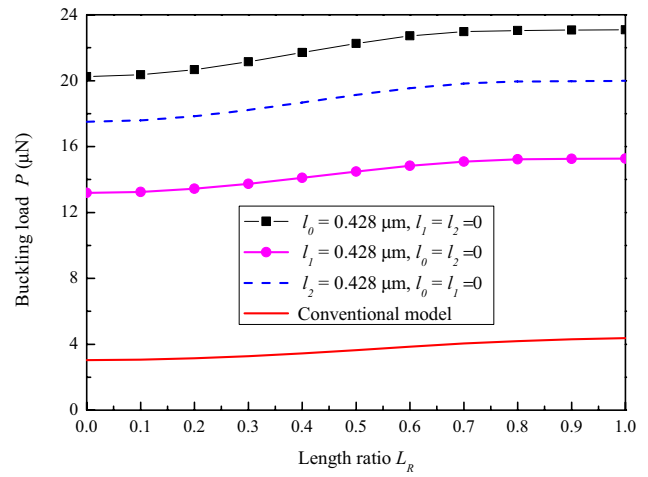
Results reveal that the general theory can be simplified as the modified couple stress theory by ignoring the deviatoric part of the strain gradients $\eta_{ijk}^{(2)}$, and the modified strain gradient elasticity theory by ignoring the symmetric part of the strain gradients η_{ijk}^s . The general theory is able to reflect the size dependency more appropriately. As the ratio of the thickness and length parameters increases, the deflection and axial displacement increase while the buckling load decreases, and thus show size effects obviously. In addition, the analysis of the contributions from the radius and thickness of the upper elastic layer on the deflection and buckling load is performed. The increase of thickness and radius of the upper elastic layer leads to the increase of the buckling load, and thus enhances the ability of the plate to resist the deformation. As the radius of the upper elastic layer increase, the bending rigidity and uniformly distributed load gradually increase. Thus, the deflection is decided by the contributions from the bending rigidity and external load. For the clamped-clamped microplate, the deflection first increases and then decreases with the increase of the radius of the upper elastic layer. The deflection achieves the maximum value when the radius ratio is 0.82 and the thickness ratio is 1.

Appendix A

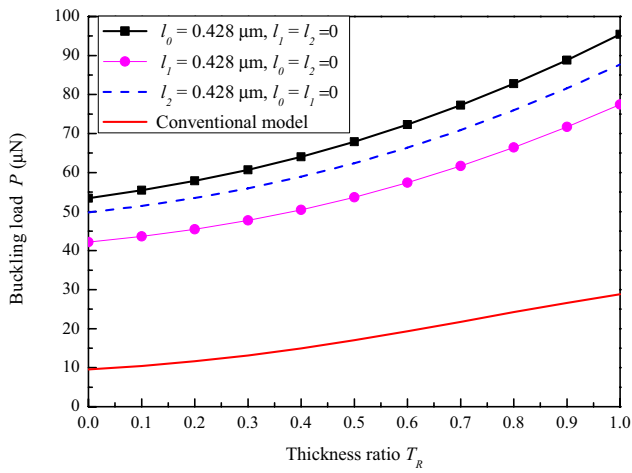
The matrix $[M(P)]$ in Eq. (74) is derived as



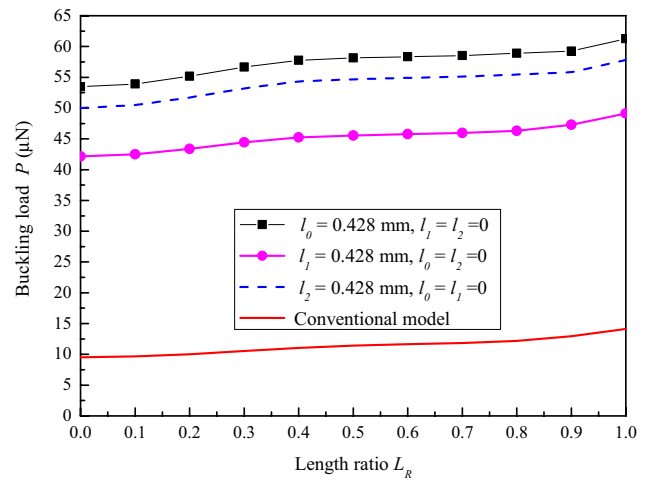
(a) Simply supported microplate



(b) Simply supported microplate



(c) Clamped-Clamped microplate



(d) Clamped-Clamped microplate

Fig. 11 Influences of the length parameters on the buckling load

$$[M(P)] = \begin{bmatrix} 1 & R^2 & m_1 & m_2 & m_3 & m_4 & 0 & 0 & 0 & 0 & 0 \\ 0 & m_5 & m_6 & m_7 & m_8 & m_9 & 0 & 0 & 0 & 0 & 0 \\ 0 & 0 & m_{10} & m_{11} & m_{12} & m_{13} & 0 & 0 & 0 & 0 & 0 \\ m_{14} & m_{15} & m_{16} & m_{17} & m_{18} & m_{19} & -1 & m_{20} & m_{21} & m_{22} & 0 \\ 0 & m_{23} & m_{24} & m_{25} & m_{26} & m_{27} & 0 & m_{28} & m_{29} & m_{30} & 0 \\ 0 & m_{31} & m_{32} & m_{33} & m_{34} & m_{35} & 0 & -2 & m_{36} & m_{37} & 0 \\ 0 & 0 & 0 & m_{38} & m_{39} & m_{40} & 0 & 0 & m_{41} & m_{42} & 0 \\ 0 & m_{43} & m_{44} & m_{45} & m_{46} & m_{47} & 0 & m_{48} & m_{49} & m_{50} & m_{51} \\ 0 & 0 & m_{52} & m_{53} & m_{54} & m_{55} & 0 & 0 & m_{56} & m_{57} & 0 \\ 0 & 0 & 0 & 0 & 0 & 0 & 0 & m_{58} & m_{59} & m_{60} & m_{61} \\ 0 & 0 & 0 & 0 & 0 & 0 & 0 & 0 & m_{62} & m_{63} & 0 \end{bmatrix}$$

with

$$\begin{aligned}
 m_1 &= \ln R & m_2 &= R^2 \ln R \\
 m_3 &= I_0(dR) & m_4 &= k_0(dR) \\
 m_5 &= -2c_{3(1)}I_1 + 2g_{7(1)}h_2 + 4A_{2(1)}h_2 \\
 m_6 &= (-2A_{1(1)} + 2A_{7(1)})/R^4 \\
 &\quad + (-c_{3(1)}I_1 + g_{7(1)}h_1 - 2g_{2(1)}h_1)/R^2 \\
 m_7 &= (6A_{1(1)} - 2A_{7(1)})/R^2 - c_{3(1)}I_1(2\ln R + 1) \\
 &\quad + g_{7(1)}h_1(2\ln R + 1) + 4A_{2(1)}(\ln R + 1) \\
 &\quad + 2g_{2(1)}h_1(2\ln R + 3) \\
 m_8 &= -\frac{1}{4}d^4A_{1(1)} + \frac{3}{2}I_0(dR) + 2I_2(dR) \\
 &\quad + \frac{1}{2}I_4(dR) - \frac{A_{1(1)}d^3}{4R}(I_3(dR) + 3I_1(dR)) \\
 &\quad + \left(\frac{1.5A_{1(1)}d^2}{R^2} - \frac{0.5A_{7(1)}d^2}{R^2} + 0.5A_{2(1)}d^2 + g_{2(1)}h_1d^2 \right) \\
 &\quad (I_0(dR) + I_2(dR)) \\
 &\quad + \left(-\frac{3A_{1(1)}d}{R^3} + \frac{A_{7(1)}d}{R^3} - \frac{c_{3(1)}I_1d}{R} \right. \\
 &\quad \left. + \frac{g_{7(1)}h_1d}{R} + \frac{dA_{2(1)}}{R} \right) I_1(dR) \\
 m_9 &= -\frac{d^4A_{1(1)}}{4} \left(\frac{3}{2}k_0(dR) + 2k_2(dR) + \frac{1}{2}k_4(dR) \right) \\
 &\quad + \frac{A_{1(1)}d^3}{4R}(3k_1(dR) + k_3(dR)) \\
 &\quad + \left(\frac{1.5A_{1(1)}d^2}{R^2} - \frac{0.5A_{7(1)}d^2}{R^2} + 0.5A_{2(1)}d^2 \right. \\
 &\quad \left. + g_{2(1)}h_1d^2 \right) (k_0(dR) + k_2(dR)) \\
 &\quad \left(\frac{3A_{1(1)}d}{R^3} - \frac{A_{7(1)}d}{R^3} + \frac{c_{3(1)}I_1d}{R} \right. \\
 &\quad \left. - \frac{g_{7(1)}h_1d}{R} - \frac{dA_{2(1)}}{R} \right) k_1(dR)
 \end{aligned}$$

(100)

$$\begin{aligned}
 m_{10} &= \frac{2A_{1(1)} - 2A_{7(1)}}{R^3} \\
 m_{11} &= \frac{2A_{1(1)} + 2A_{7(1)}}{R} \\
 m_{12} &= \frac{A_{1(1)}d^3}{4}(3I_1(dR) + I_3(dR)) \\
 &\quad + \frac{A_{7(1)}d^2}{2R}(I_0(dR) + I_2(dR)) \\
 &\quad + \frac{-A_{7(1)}d}{R^2}I_1(dR) \\
 m_{13} &= \frac{A_{1(1)}d^3}{4}(-3k_1(dR) - k_3(dR)) \\
 &\quad + \frac{A_{7(1)}d^2}{2R}(k_0(dR) + k_2(dR)) + \frac{A_{7(1)}d}{R^2}k_1(dR) \\
 m_{14} &= 1 & m_{15} &= R_1^2 & m_{16} &= \ln R_1 \\
 m_{17} &= R_1^2 \ln R_1 & m_{18} &= I_0(dR_1) & m_{19} &= k_0(dR_1) \\
 m_{20} &= -R_1^2 & m_{21} &= -J_0(\sqrt{s_1}R_1) \\
 m_{22} &= -J_0(\sqrt{s_2}R_1) & m_{23} &= 2R_1 & m_{24} &= \frac{1}{R_1} \\
 m_{25} &= 2R_1 \ln R_1 + R_1 & m_{26} &= dI_1(dR_1) \\
 m_{27} &= -dk_1(dR_1) & m_{28} &= -2R_1 \\
 m_{29} &= \sqrt{s_1}J_1(\sqrt{s_1}R_1) \\
 m_{30} &= \sqrt{s_2}J_1(\sqrt{s_2}R_1) & m_{31} &= 2 & m_{32} &= -\frac{1}{R_1^2} \\
 m_{33} &= 2\ln R_1 + 3 & m_{34} &= \frac{d^2}{2}(I_0(dR_1) + I_2(dR_1)) \\
 m_{35} &= \frac{d^2}{2}(k_0(dR_1) + k_2(dR_1)) \\
 m_{36} &= \frac{s_1}{2}J_0(\sqrt{s_1}R_1) - J_2(\sqrt{s_1}R_1) \\
 m_{37} &= \frac{s_2}{2}J_0(\sqrt{s_2}R_1) - J_2(\sqrt{s_2}R_1) \\
 m_{38} &= \frac{4A_{2(1)}}{R_1} \\
 m_{39} &= \frac{d^5A_{1(1)}}{4} \left(\frac{5}{2}I_1(dR_1) + \frac{5}{4}I_3(dR_1) + \frac{1}{4}I_5(dR_1) \right) \\
 &\quad + \left(\frac{-3A_{1(1)}}{R_1^4} + \frac{dA_{2(1)}}{R_1^2} \right) I_1(dR_1) \\
 &\quad + \left(\frac{3A_{1(1)}d^2}{2R_1^3} - \frac{A_{2(1)}d^2}{2R_1} \right) (I_0(dR_1) + I_2(dR_1)) \\
 &\quad + \left(\frac{-3A_{1(1)}d^3}{4R_1^2} + \frac{-A_{2(1)}d^3}{4} \right) (3I_1(dR_1) + I_3(dR_1)) \\
 &\quad + \frac{A_{1(1)}d^4}{2R_1} \left(\frac{3}{2}I_0(dR_1) + 2I_2(dR_1) + \frac{1}{2}I_4(dR_1) \right) \\
 m_{40} &= \frac{A_{1(1)}d^5}{4} \left(-\frac{5}{2}k_1(dR_1) - \frac{5}{4}k_3(dR_1) \right) \\
 &\quad - \frac{1}{4}k_5(dR_1) + \left(\frac{3A_{1(1)}d}{R_1^4} - \frac{A_{2(1)}d}{R_1^2} \right) \\
 &\quad k_1(dR_1) + \left(\frac{3A_{1(1)}d^2}{2R_1^3} - \frac{A_{2(1)}d^2}{2R_1} \right) \\
 &\quad (k_0(dR_1) + k_2(dR_1)) + \left(\frac{3A_{1(1)}d^3}{4R_1^2} + \frac{A_{2(1)}d^3}{4} \right) \\
 &\quad (3k_1(dR_1) + k_3(dR_1)) + \frac{A_{1(1)}d^4}{2R_1} \\
 &\quad \left(\frac{3}{2}k_0(dR_1) + 2k_2(dR_1) + \frac{1}{2}k_4(dR_1) \right)
 \end{aligned}$$

(101)

$$\begin{aligned}
 m_{41} = & -0.5(A_3s_1^{2.5}m - A_1s_1^{2.5})\left(\frac{5}{4}J_1(\sqrt{s_1}R_1) \right. \\
 & - \frac{5}{8}J_3(\sqrt{s_1}R_1) + \frac{1}{8}J_5(\sqrt{s_1}R_1) \left. \right) \\
 & - \left(\frac{3A_1\sqrt{s_1}}{R_1^4} - \frac{3A_3\sqrt{s_1}m}{R_1^4} - \frac{A_2\sqrt{s_1}}{R_1^2} + \frac{A_4\sqrt{s_1}m}{R_1^2} \right) \\
 & J_1(\sqrt{s_1}R_1) - \left(\frac{-3A_1s_1}{2R_1^3} + \frac{3A_3s_1m}{2R_1^3} + \frac{A_2s_1}{2R_1} - \frac{A_4s_1m}{2R_1} \right) \\
 & (J_0(\sqrt{s_1}R_1) - J_2(\sqrt{s_1}R_1)) \\
 & - \left(\frac{3A_1s_1^{0.5}}{2R_1^2} - \frac{3A_3s_1^{1.5}m}{2R_1^2} + \frac{A_2s_1^{1.5}}{2} - \frac{A_4s_1^{1.5}m}{2} \right) \\
 & (-1.5J_1(\sqrt{s_1}R_1) + 0.5J_3(\sqrt{s_1}R_1)) \\
 & - \left(-\frac{A_1s_1^2m}{R_1} + \frac{A_3s_1^2m}{R_1} \right) \\
 & \left(-\frac{3}{4}J_0(\sqrt{s_1}R_1) + J_2(\sqrt{s_1}R_1) - \frac{1}{4}J_4(\sqrt{s_1}R_1) \right) \tag{102}
 \end{aligned}$$

$$\begin{aligned}
 m_{42} = & -(-0.5(A_1s_2^{2.5}m + A_3s_2^{2.5}n) \\
 & \left(\frac{5}{4}J_1(\sqrt{s_2}R_1) - \frac{5}{8}J_3(\sqrt{s_2}R_1) + \frac{1}{8}J_5(\sqrt{s_2}R_1) \right) \\
 & - \left(\frac{3A_1\sqrt{s_2}}{R_1^4} - \frac{3A_3\sqrt{s_2}n}{R_1^4} - \frac{A_2\sqrt{s_2}n}{R_1^2} + \frac{A_4\sqrt{s_2}n}{R_1^2} \right) \\
 & J_1(\sqrt{s_2}R_1) - \left(\frac{-3A_1s_2}{2R_1^3} + \frac{3A_3s_2n}{2R_1^3} + \frac{A_2s_2}{2R_1} - \frac{A_4s_2n}{2R_1} \right) \\
 & (J_0(\sqrt{s_2}R_1) - J_2(\sqrt{s_2}R_1)) \\
 & - \left(\frac{3A_1s_2^{1.5}}{2R_1^2} - \frac{3A_3s_2^{1.5}n}{2R_1^2} + \frac{A_2s_2^{1.5}}{2} - \frac{A_4s_2^{1.5}n}{2} \right) \\
 & (1.5J_1(\sqrt{s_2}R_1) + 0.5J_3(\sqrt{s_2}R_1)) \\
 & - \left(-\frac{A_1s_2^2}{R_1} + \frac{A_3s_2^2n}{R_1} \right) \\
 & \left(-\frac{3}{4}J_0(\sqrt{s_2}R_1) + J_2(\sqrt{s_2}R_1) - \frac{1}{4}J_4(\sqrt{s_2}R_1) \right) \tag{103}
 \end{aligned}$$

$$\begin{aligned}
 m_{43} = & -2c_{3(1)}I_{(1)} + 2g_{7(1)}h_{(1)} + 4A_{2(1)} + 4g_{2(1)}h_{(1)} \\
 m_{44} = & \frac{-2A_{1(1)} + 2A_{7(1)}}{R_1^4} \\
 & + \frac{-c_{3(1)}I_{(1)} + g_{7(1)}h_{(1)} - 2g_{2(1)}h_{(1)}}{R_1^2} \tag{104}
 \end{aligned}$$

$$\begin{aligned}
 m_{45} = & \frac{6A_{1(1)} - 2A_{7(1)}}{R_1^2} - c_{3(1)}I_{(1)}(2\ln(R_1) + 1) \\
 & + g_{7(1)}h_{(1)}(2\ln(R_1) + 1) \\
 & + 4A_{2(1)}(2\ln(R_1) + 1) + 2g_{2(1)}h_{(1)}(2\ln(R_1) + 3)
 \end{aligned}$$

$$\begin{aligned}
 m_{46} = & \frac{-d^4A_{1(1)}}{4} \left(\frac{3}{2}I_0(dR_1) + 2I_2(dR_1) \right) \\
 & + \frac{1}{2}I_4(dR_1) + \frac{d^3A_{1(1)}}{4R_1} (3I_1(dR_1) + I_3(dR_1)) \\
 & + \left(\frac{1.5A_{1(1)}d^2}{R_1^2} - \frac{0.5A_{7(1)}d^2}{R_1^2} + 0.5A_{2(1)}d^2 + g_{2(1)}h_1d^2 \right) \\
 & (I_0(dR_1) + I_2(dR_1)) \\
 & + \left(-\frac{3A_{1(1)}d}{R_1^3} + \frac{A_{7(1)}d}{R_1^3} - \frac{c_{3(1)}I_{(1)}d}{R_1} \right. \\
 & \left. + \frac{g_{7(1)}h_{(1)}d}{R_1} + \frac{A_{2(1)}d}{R_1} \right) I_1(dR_1) \tag{105}
 \end{aligned}$$

$$\begin{aligned}
 m_{47} = & \frac{-d^4A_{1(1)}}{4} \left(\frac{3}{2}k_0(dR_1) + 2k_2(dR_1) + \frac{1}{2}k_4(dR_1) \right) \\
 & + \frac{d^3A_{1(1)}}{4R_1} (3k_1(dR_1) + k_3(dR_1)) \\
 & + \left(\frac{1.5A_{1(1)}d^2}{R_1^2} - \frac{0.5A_{7(1)}d^2}{R_1^2} + 0.5A_{2(1)}d^2 + g_{2(1)}h_1d^2 \right) \\
 & (k_0(dR_1) + k_2(dR_1)) \\
 & + \left(-\frac{3A_{1(1)}d}{R_1^3} - \frac{A_{7(1)}d}{R_1^3} + \frac{c_{3(1)}I_1d}{R_1} - \frac{g_{7(1)}h_{(1)}d}{R_1} - \frac{A_{2(1)}d}{R_1} \right) k_1(dR_1) \tag{106}
 \end{aligned}$$

$$\begin{aligned}
 m_{48} = & 2(c_{3(1)}I_{(1)} + c_{3(2)}I_{(2)}) - 2(g_{7(1)}h_{(1)} + g_{7(2)}h_{(2)}) \\
 & - 4(g_{2(1)}h_{(1)} + g_{2(2)}h_{(2)}) - 4A_2 \\
 m_{49} = & -\frac{A_1s_1^2m}{2} \left(-\frac{3}{4}J_0(\sqrt{s_1}R_1) + J_2(\sqrt{s_1}R_1) - \frac{1}{4}J_4(\sqrt{s_1}R_1) \right) \\
 & - \frac{A_{(1)}s_1^{1.5} - A_{(1)}s_1^{1.5}m}{2R_1} \left(-\frac{3}{2}J_1(\sqrt{s_1}R_1) + \frac{1}{2}J_3(\sqrt{s_1}R_1) \right) \\
 & - \left(\frac{-3A_{(1)}s_1 + 3A_{(3)}s_1m}{2R_1^2} + \frac{A_{(7)}s_1 - A_{(8)}s_1m}{2R_1^2} \right. \\
 & \left. - (g_{2(1)}h_{(1)} + g_{2(2)}h_{(2)})s_1 - \frac{A_{(2)}s_1}{2} + \frac{A_{(4)}s_1m}{2} \right) \\
 & (J_0(\sqrt{s_1}R_1) - J_2(\sqrt{s_1}R_1)) \\
 & - \left(\frac{3A_1\sqrt{s_1} - 3A_3\sqrt{s_1}m}{R_1^3} + \frac{-A_7\sqrt{s_1} + A_8\sqrt{s_1}m}{R_1^3} \right. \\
 & + \frac{(c_{3(1)}I_{(1)} + c_{3(2)}I_{(2)})\sqrt{s_1}}{R_1} - \frac{(g_{7(1)}h_{(1)} + g_{7(2)}h_{(2)})\sqrt{s_1}}{R_1} \\
 & \left. - \frac{(c_{3(1)}S_{(1)} + c_{3(2)}S_{(2)})\sqrt{s_1}m}{R_1} - \frac{A_2\sqrt{s_1}}{R_1} + \frac{A_4\sqrt{s_1}m}{R_1} \right) J_1(\sqrt{s_1}R_1) \tag{107}
 \end{aligned}$$

$$\begin{aligned}
 m_{50} = & -\frac{A_1 s_2^2 - A_3 s_2^2 n}{2} \left(-\frac{3}{4} J_0(\sqrt{s_2} R_1) + J_2(\sqrt{s_2} R_1) \right. \\
 & - \frac{1}{4} J_4(\sqrt{s_2} R_1) \left. \right) - \frac{A_{(1)} s_2^{1.5} - A_{(3)} s_2^{1.5} n}{2R_1} \\
 & \left(-\frac{3}{2} J_1(\sqrt{s_2} R_1) + \frac{1}{2} J_3(\sqrt{s_2} R_1) \right) \\
 & - \left(\frac{-3A_{(1)} s_2 + 3A_{(3)} s_2 m}{2R_1^2} + \frac{A_{(7)} s_2 - A_{(8)} s_2 n}{2R_1^2} \right. \\
 & \left. - (g_{2(1)} h_{(1)} + g_{2(2)} h_{(2)}) s_2 - \frac{A_{(2)} s_2}{2} + \frac{A_{(4)} s_2 n}{2} \right) \\
 & (J_0(\sqrt{s_2} R_1) - J_2(\sqrt{s_2} R_1)) \\
 & - \left(\frac{3A_1 \sqrt{s_2} - 3A_3 \sqrt{s_2} n}{R_1^3} + \frac{-A_7 \sqrt{s_2} + A_8 \sqrt{s_2} n}{R_1^3} \right. \\
 & + \frac{(c_{3(1)} I_{(1)} + c_{3(2)} I_{(2)}) \sqrt{s_2}}{R_1} - \frac{(g_{7(1)} h_{(1)} + g_{7(2)} h_{(2)}) \sqrt{s_2}}{R_1} \\
 & - \frac{(c_{3(1)} S_{(1)} + c_{3(2)} S_{(2)}) \sqrt{s_2} m}{R_1} \\
 & \left. - \frac{A_2 \sqrt{s_2}}{R_1} + \frac{A_4 \sqrt{s_2} n}{R_1} \right) J_1(\sqrt{s_2} R_1)
 \end{aligned} \tag{108}$$

$$m_{51} = -2(c_{3(1)} S_{(1)} + c_{3(2)} S_{(2)}) - 4A_4$$

$$m_{52} = \frac{2A_{1(1)} - 2A_{7(1)}}{R_1^3}$$

$$m_{53} = \frac{2A_{1(1)} + 2A_{7(1)}}{R_1}$$

$$\begin{aligned}
 m_{54} = & \frac{A_{1(1)} d^3}{4} (3I_1(dR_1) + I_3(dR_1)) \\
 & + \frac{A_{7(1)} d^2}{2R_1} (I_0(dR_1) + I_2(dR_1)) \\
 & - \frac{A_{7(1)} d}{R_1^2} I_1(dR_1)
 \end{aligned}$$

$$\begin{aligned}
 m_{55} = & \frac{A_{1(1)} d^3}{4} (-3k_1(dR_1) - k_3(dR_1)) \\
 & + \frac{A_{7(1)} d^2}{2R_1} (k_0(dR_1) + k_2(dR_1)) \\
 & + \frac{A_{7(1)} d}{R_1^2} k_1(dR_1)
 \end{aligned} \tag{109}$$

$$\begin{aligned}
 m_{56} = & -\left(\frac{-A_{(1)} s_1^{1.5} + A_{(3)} s_1^{1.5} m}{2} \right. \\
 & \left(-\frac{3}{2} J_1(\sqrt{s_1} R_1) + \frac{1}{2} J_3(\sqrt{s_1} R_1) \right) \\
 & - \left(\frac{A_{(8)} s_1 m - A_{(7)} s_1}{2R_1} (J_0(\sqrt{s_1} R_1) - J_2(\sqrt{s_1} R_1)) \right. \\
 & \left. - \frac{A_7 \sqrt{s_1} - A_8 \sqrt{s_1} m}{R_1^2} \right) \\
 & J_1(\sqrt{s_1} R_1)
 \end{aligned}$$

$$\begin{aligned}
 m_{57} = & -\left(\frac{-A_{(1)} s_2^{1.5} + A_{(3)} s_2^{1.5} n}{2} \right. \\
 & \left(-\frac{3}{2} J_1(\sqrt{s_2} R_1) + \frac{1}{2} J_3(\sqrt{s_2} R_1) \right) \\
 & - \left(\frac{A_{(8)} s_2 n - A_{(7)} s_2}{2R_1} (J_0(\sqrt{s_2} R_1) - J_2(\sqrt{s_2} R_1)) \right. \\
 & \left. - \frac{A_7 \sqrt{s_2} - A_8 \sqrt{s_2} n}{R_1^2} \right) \\
 & J_1(\sqrt{s_2} R_1)
 \end{aligned} \tag{110}$$

$$\begin{aligned}
 m_{58} = & \frac{-A_3 s_1^2 + A_5 s_1^2 m}{2} \\
 & \left(-\frac{3}{4} J_0(\sqrt{s_1} R_1) + J_2(\sqrt{s_1} R_1) - \frac{1}{4} J_4(\sqrt{s_1} R_1) \right) \\
 & + \frac{-A_3 s_1^{1.5} + A_5 s_1^{1.5} m}{2R_1} \\
 & \left(-\frac{3}{2} J_1(\sqrt{s_1} R_1) + \frac{1}{2} J_3(\sqrt{s_1} R_1) \right) \\
 & + \left(\frac{3A_{(3)} s_1 - 3A_5 s_1 m}{2R_1^2} \right. \\
 & \left. + \frac{-A_8 s_1 + A_9 s_1 m}{2R_1^2} + \frac{A_4 s_1}{2} - \frac{A_6 s_1 m}{2} \right) \\
 & (J_0(\sqrt{s_1} R_1) - J_2(\sqrt{s_1} R_1)) \\
 & + \left(\frac{-3A_3 s_1^{0.5} + 3A_5 s_1^{0.5} m}{R_1^3} + \frac{A_8 s_1^{0.5} - A_9 s_1^{0.5} m}{R_1^3} \right. \\
 & - \frac{(c_{3(1)} S_{(1)} + c_{3(2)} S_{(2)}) \sqrt{s_1}}{R_1} + \frac{(c_{3(1)} h_{(1)} + c_{3(2)} h_{(2)}) \sqrt{s_1} m}{R_1} \\
 & \left. + \frac{A_4 \sqrt{s_1}}{R_1} - \frac{A_6 \sqrt{s_1} m}{R_1} \right) J_1(\sqrt{s_1} R_1)
 \end{aligned} \tag{111}$$

$$\begin{aligned}
 m_{59} = & \frac{-A_3s_2^2 + A_5s_2^2n}{2} \\
 & \left(-\frac{3}{4}J_0(\sqrt{s_2}R_1) + J_2(\sqrt{s_2}R_1) - \frac{1}{4}J_4(\sqrt{s_2}R_1) \right) \\
 & + \frac{-A_3s_2^{1.5} + A_5s_2^{1.5}n}{2R_1} \left(-\frac{3}{2}J_1(\sqrt{s_2}R_1) + \frac{1}{2}J_3(\sqrt{s_2}R_1) \right) \\
 & + \left(\frac{3A_{(3)}s_2 - 3A_5s_2m}{2R_1^2} + \frac{-A_8s_2 + A_9s_2n}{2R_1^2} \right. \\
 & + \left. \frac{A_4s_2}{2} - \frac{A_6s_2n}{2} \right) (J_0(\sqrt{s_2}R_1) - J_2(\sqrt{s_2}R_1)) \\
 & + \left(\frac{-3A_3s_2^{0.5} + 3A_5s_2^{0.5}m}{R_1^3} + \frac{A_8s_2^{0.5} - A_9s_2^{0.5}m}{R_1^3} \right. \\
 & - \frac{(c_{3(1)}S_{(1)} + c_{3(2)}S_{(2)})\sqrt{s_2}}{R_1} + \frac{(c_{3(1)}h_{(1)} + c_{3(2)}h_{(2)})\sqrt{s_2}n}{R_1} \\
 & \left. + \frac{A_4\sqrt{s_2}}{R_1} - \frac{A_6\sqrt{s_2}n}{R_1} \right) J_1(\sqrt{s_2}R_1)
 \end{aligned} \tag{112}$$

$$m_{60} = 2(c_{3(1)}S_{(1)} + c_{3(2)}S_{(2)}) - 4A_4$$

$$m_{61} = 4A_6 - 2(c_{3(1)}h_{(1)} + c_{3(2)}h_{(2)})$$

$$\begin{aligned}
 m_{62} = & \frac{A_{(3)}s_1^{1.5} - A_5s_1^{1.5}m}{2} \\
 & \left(-\frac{3}{2}J_1(\sqrt{s_1}R_1) + \frac{1}{2}J_3(\sqrt{s_1}R_1) + \frac{A_8s_1 - A_9s_1m}{2R_1} \right. \\
 & (J_0(\sqrt{s_1}R_1) - J_2(\sqrt{s_1}R_1)) \\
 & \left. + \left(\frac{-A_8\sqrt{s_1} + A_9\sqrt{s_1}m}{R_1^2} \right) J_1(\sqrt{s_1}R_1) \right)
 \end{aligned} \tag{113}$$

$$\begin{aligned}
 m_{63} = & \frac{A_{(3)}s_2^{1.5} - A_5s_2^{1.5}n}{2} \\
 & \left(-\frac{3}{2}J_1(\sqrt{s_2}R_1) + \frac{1}{2}J_3(\sqrt{s_2}R_1) + \frac{A_8s_2 - A_9s_2n}{2R_1} \right. \\
 & (J_0(\sqrt{s_2}R_1) - J_2(\sqrt{s_2}R_1)) \\
 & \left. + \left(\frac{-A_8\sqrt{s_2} + A_9\sqrt{s_2}n}{R_1^2} \right) J_1(\sqrt{s_2}R_1) \right)
 \end{aligned} \tag{114}$$

The vector D in Eq. (74) is given as

$$[D] = [0 \ 0 \ 0 \ m_{64} \ m_{65} \ m_{66} \ m_{67} \ m_{68} \ m_{69} \ m_{70} \ m_{71}]$$

with

$$\begin{aligned}
 m_{64} = & t_0R_1^4 \quad m_{65} = 4t_0R_1^3 \\
 m_{66} = & 12t_0R_1^2 \quad m_{67} = -32A_2t_0R_1 + 8A_4t_1R_1 \\
 m_{68} = & -24A_1t_0 + 6A_3t_1 + 2A_8t_1 - 8A_7t_0 - (c_{3(1)}I_{(1)} \\
 & + c_{3(2)}I_{(2)})4R_1^2t_0 \\
 & + (g_{7(2)}h_2 + g_{7(1)}h_1)4R_1^2t_0 + (c_{3(2)}S_2 + c_{3(1)}S_1)R_1^2t_1 \\
 & + 24t_0(g_{2(2)}h_2 + g_{2(1)}h_1)R_1^2 \\
 & + 16t_0R_1^2A_2 - 16t_3R_1^2A_4 \\
 m_{69} = & 24t_0R_1A_1 + 8t_0R_1A_7 - 6t_1R_1A_3 - 2t_1R_1A_8 \\
 m_{70} = & -24A_3t_0 + 6A_5t_1 - 8A_8t_0 + 2A_9t_1 \\
 & - (c_{3(2)}S_{(2)} + c_{3(1)}S_{(1)})4R_1^2t_0 \\
 & + (c_{3(2)}h_2 + c_{3(1)}h_1)R_1^2t_1 + 16t_0R_1^2A_4 - 16t_3R_1^2A_6 \\
 m_{71} = & 24t_0R_1A_3 + 8t_0R_1A_8 - 6t_1R_1A_5 - 2t_1R_1A_9 \\
 t_0 = & \frac{qA_6}{64(A_2A_6 - A_4^2)} \\
 t_1 = & \frac{qA_4}{16(A_2A_6 - A_4^2)} \\
 t_3 = & \frac{qA_4}{64(A_2A_6 - A_4^2)}
 \end{aligned} \tag{115}$$

Acknowledgements This work was supported by the Natural Science Foundation of Shandong Province of China (ZR2021QA078), Taishan Scholars Program of Shandong Province (tsqn20190401, tsqn201909108), the Natural Science Foundation of Shandong Province of China (ZR2020ME164, ZR2021MF042), the Key Research and Development Project of Zibo City (2020SNPT0088), the Open Fund of State Key Laboratory of Applied Optics (SKLAO2020001A16) and the Shandong Provincial Key Laboratory of Precision Manufacturing and Non-traditional Machining.

Declarations

Conflicts of interest The authors declare that they have no known competing financial interests or personal relationships that could have appeared to influence the work reported in this paper.

References

1. Hamlehdar M, Kasaiean A, Safaei MR (2019) Energy harvesting from fluid flow using piezoelectrics: a critical review. *Renew Energy* 143:1826–1838
2. Liu H, Zhong J, Lee C et al (2018) A comprehensive review on piezoelectric energy harvesting technology: materials, mechanisms, and applications. *Appl Phys Rev* 5(4):041306
3. Baz A (2019) Active acoustic metamaterial with tunable effective density using a disturbance rejection controller. *J Appl Phys* 125(7):074503
4. Afzal MS, Shim H, Roh Y (2018) Design of a piezoelectric multilayered structure for ultrasound sensors using the equivalent circuit method. *Sensors* 18:12

5. Nguyen VT, Kumar P, Leong JYC (2018) Finite element modelling and simulations of piezoelectric actuators responses with uncertainty quantification. *Computation* 6(4):60
6. Prasad SAN, Gallas Q, Horowitz S et al (2006) Analytical electroacoustic model of a piezoelectric composite circular plate. *AIAA J* 44(10):2311–2318
7. Bakhtiari-Shahri M, Moeinfard H (2019) Optimal design of a stable fuzzy controller for beyond pull-in stabilization of electrostatically actuated circular microplates. *J Vib Acoust* 141(1):011019.1–011019.9
8. Wang T, He J, Wang J, et al (2018) Numerical and Experimental Study of Valve-Less Micropump Using Dynamic Multiphysics Model. In: 2018 IEEE 13th annual international conference on nano/micro engineered and molecular systems (NEMS). IEEE, pp 300–303
9. Shahri MB, Moeinfard H (2019) Energy harvesting from unimorph piezoelectric circular plates under random acoustic and base acceleration excitations. *Mech Syst Signal Process* 130:502–523
10. Chen S, Xie X, Kan J et al (2019) A hydraulic-driven piezoelectric pump with separable channel for drug delivery. *Sens Actuat A* 295:210–216
11. Hu Y, Liang X, Wang W (2017) Deflection of circular diaphragm-type piezoactuators coupling with gas compression in micropumps. *Microsyst Technol* 23(12):5329–5341
12. Yuan TC, Yang J, Chen LQ (2019) Nonlinear vibration analysis of a circular composite plate harvester via harmonic balance. *Acta Mech Sin* 35(4):912–925
13. Sahoo SR, Ray MC (2019) Active damping of geometrically nonlinear vibrations of smart composite plates using elliptical SCLD treatment with fractional derivative viscoelastic layer. *Eur J Mech A/Solids* 78:103823
14. Sun W, Jo S, Seok J (2019) Development of the optimal bluff body for wind energy harvesting using the synergetic effect of coupled vortex induced vibration and galloping phenomena. *Int J Mech Sci* 156:435–445
15. Chong SV, Williams GVM (2019) Magnetolectric effect in magnetostrictive-piezoelectric composites containing magnetite nanoparticles. *Sens Actuat A* 288:101–106
16. Lam DCC, Yang F, Chong ACM et al (2003) Experiments and theory in strain gradient elasticity. *J Mech Phys Solids* 51(8):1477–1508
17. Li Z, He Y, Zhang B et al (2019) Experimental investigation and theoretical modelling on nonlinear dynamics of cantilevered microbeams. *Eur J Mech A/Solids* 78:103834
18. Akgöz B, Civalek Ö (2013) Buckling analysis of functionally graded microbeams based on the strain gradient theory. *Acta Mech* 224(9):2185–2201
19. Toupin R (1962) Elastic materials with couple-stresses. *Arch Ration Mech Anal* 11(1):385–414
20. Mindlin RD, Tiersten HF (1962) Effects of couple-stresses in linear elasticity. *Arch Ration Mech Anal* 11(1):415–448
21. Yang F, Chong ACM, Lam DCC et al (2002) Couple stress based strain gradient theory for elasticity. *Int J Solids Struct* 39(10):2731–2743
22. Hadjesfandiari AR, Dargush GF (2011) Couple stress theory for solids. *Int J Solids Struct* 48(18):2496–2510
23. Neff P, Jeong J (2009) A new paradigm: the linear isotropic Cosserat model with conformally invariant curvature energy. *ZAMM J Appl Math Mech* 89(2):107
24. Mindlin RD (1964) Micro-structure in linear elasticity. *Arch Ration Mech Anal* 16(1):51–78
25. Münch I, Neff P, Madeo A et al (2017) The modified indeterminate couple stress model: why Yang et al.'s arguments motivating a symmetric couple stress tensor contain a gap and why the couple stress tensor may be chosen symmetric nevertheless. *ZAMM-J Appl Math Mech* 97(12):1524–1554
26. Neff P, Münch I, Ghiba ID et al (2016) On some fundamental misunderstandings in the indeterminate couple stress model. A comment on recent papers of AR Hadjesfandiari and GF Dargush. *Int J Solids Struct* 81:233–243
27. Mindlin RD, Eshel NN (1968) On first strain-gradient theories in linear elasticity. *Int J Solids Struct* 4(1):109–124
28. Aifantis EC (1992) On the role of gradients in the localization of deformation and fracture. *Int J Eng Sci* 30(10):1279–1299
29. Zhou S, Li A, Wang B (2016) A reformulation of constitutive relations in the strain gradient elasticity theory for isotropic materials. *Int J Solids Struct* 80:28–37
30. Polizzotto C (2013) A second strain gradient elasticity theory with second velocity gradient inertia-part I: constitutive equations and quasi-static behavior. *Int J Solids Struct* 50(24):3749–3765
31. Zhao B, Liu T, Chen J et al (2019) A new Bernoulli-Euler beam model based on modified gradient elasticity. *Arch Appl Mech* 89(2):277–289
32. Fu G, Zhang Z, Fu J et al (2022) On the strain gradient effects on buckling of the partially covered laminated microbeam. *Appl Math Model* 102:472–491
33. Yue YM, Xu KY, Tan ZQ et al (2019) The influence of surface stress and surface-induced internal residual stresses on the size-dependent behaviors of Kirchhoff microplate. *Arch Appl Mech* 89(7):1301–1315
34. Barretta R, Faghidian SA, De Sciarra FM (2019) Stress-driven nonlocal integral elasticity for axisymmetric nano-plates. *Int J Eng Sci* 136:38–52
35. Mohammadi M, Mohseni E, Moeinfar M (2019) Bending, buckling and free vibration analysis of incompressible functionally graded plates using higher order shear and normal deformable plate theory. *Appl Math Model* 69:47–62
36. Thai CH, Ferreira AJM, Rabczuk T et al (2018) Size-dependent analysis of FG-CNTRC microplates based on modified strain gradient elasticity theory. *Eur J Mech A/Solids* 72:521–538
37. Akgöz B, Civalek Ö (2015) A novel microstructure-dependent shear deformable beam model. *Int J Mech Sci* 99:10–20
38. Akgöz B, Civalek Ö (2014) Longitudinal vibration analysis for microbars based on strain gradient elasticity theory. *J Vib Control* 20(4):606–616
39. Ebrahimi F, Barati MR, Civalek Ö (2020) Application of Chebyshev-Ritz method for static stability and vibration analysis of nonlocal microstructure-dependent nanostructures. *Eng Comput* 36(3):953–964
40. Farzam A, Hassani B (2019) Size-dependent analysis of FG microplates with temperature-dependent material properties using modified strain gradient theory and isogeometric approach. *Compos B Eng* 161:150–168
41. Shahrbabaki EA (2018) On three-dimensional nonlocal elasticity: free vibration of rectangular nanoplate. *Eur J Mech A/Solids* 71:122–133
42. Alizadeh M, Fattahi AM (2019) Non-classical plate model for FGMs. *Eng Comput* 35(1):215–228
43. Li M, Soares CG, Yan R (2021) Free vibration analysis of FGM plates on Winkler/Pasternak/Kerr foundation by using a simple quasi-3D HSDT. *Compos Struct* 264:113643
44. Nguyen HX, Atroshchenko E, Ngo T et al (2019) Vibration of cracked functionally graded microplates by the strain gradient theory and extended isogeometric analysis. *Eng Struct* 187:251–266
45. Quintana MV, Raffo JL (2019) A variational approach to vibrations of laminated composite plates with a line hinge. *Eur J Mech A/Solids* 73:11–21
46. Thanh CL, Tran LV, Vu-Huu T et al (2019) Size-dependent nonlinear analysis and damping responses of FG-CNTRC microplates. *Comput Methods Appl Mech Eng* 353:253–276

47. Li A, Ji X, Zhou S et al (2021) Nonlinear axisymmetric bending analysis of strain gradient thin circular plate. *Appl Math Model* 89:363–380
48. Zhou YF, Wang ZM (2019) Dynamic instability of axially moving viscoelastic plate. *Eur J Mech A/Solids* 73:1–10
49. Akgöz B, Civalek Ö (2015) A microstructure-dependent sinusoidal plate model based on the strain gradient elasticity theory. *Acta Mech* 226(7):2277–2294
50. Ullah S, Zhong Y, Zhang J (2019) Analytical buckling solutions of rectangular thin plates by straightforward generalized integral transform method. *Int J Mech Sci* 152:535–544
51. Ansari R, FaghihShojaei M, Mohammadi V et al (2014) Size-dependent vibrations of post-buckled functionally graded Mindlin rectangular microplates. *Latin Am J Solids Struct* 11(13):2351–2378
52. Zenkour AM, Aljadani MH (2019) Porosity effect on thermal buckling behavior of actuated functionally graded piezoelectric nanoplates. *Eur J Mech A/Solids* 78:103835
53. Tenenbaum J, Deutsch A, Eisenberger M (2019) Analytical buckling loads for corner supported rectangular orthotropic and symmetrically laminated plates. *ZAMM-J Appl Math Mech* 99(11):e201900142
54. Arefi M, Kiani M, Rabczuk T (2019) Application of nonlocal strain gradient theory to size dependent bending analysis of a sandwich porous nanoplate integrated with piezomagnetic face-sheets. *Compos B Eng* 168:320–333
55. Chen W, Wang Y (2016) A model of composite laminated Reddy plate of the global-local theory based on new modified couple-stress theory. *Mech Adv Mater Struct* 23(6):636–651
56. Ghorbanpour Arani A, Zamani MH (2019) Investigation of electric field effect on size-dependent bending analysis of functionally graded porous shear and normal deformable sandwich nanoplate on silica Aerogel foundation. *J Sandwich Struct Mater* 21(8):2700–2734
57. Gao F, Sun W (2019) Nonlinear finite element modeling and vibration analysis of the blisk deposited strain-dependent hard coating. *Mech Syst Signal Process* 121:124–143
58. Mohammadimehr M, Emdadi M, Afshari H et al (2018) Bending, buckling and vibration analyses of MSGT microcomposite circular-annular sandwich plate under hydro-thermo-magneto-mechanical loadings using DQM. *Int J Smart Nano Mater* 9(4):233–260
59. Basak S, Raman A, Garimella SV (2005) Dynamic response optimization of piezoelectrically excited thin resonant beams. *J Vib Acoust* 127(1):18–27
60. Morris CJ, Forster FK (2000) Optimization of a circular piezoelectric bimorph for a micropump driver. *J Micromech Microeng* 10(3):459
61. Zhang J, Zhao Q, Ullah S et al (2021) A new analytical solution of vibration response of orthotropic composite plates with two adjacent edges rotationally-restrained and the others free. *Compos Struct* 2021:113882
62. Nguyen NV, Lee J, Nguyen-Xuan H (2019) Active vibration control of GPLs-reinforced FG metal foam plates with piezoelectric sensor and actuator layers. *Compos B Eng* 172:769–784
63. Roque CMC, Grasa J (2021) Geometrically nonlinear analysis of laminated composite plates using RBF-PS meshless method. *Compos Struct* 2021:113830
64. Zuo W, Li P, Du J et al (2019) Thermoelastic damping in trilayered microplate resonators. *Int J Mech Sci* 151:595–608
65. Nematollahi MS, Mohammadi H (2019) Geometrically nonlinear vibration analysis of sandwich nanoplates based on higher-order nonlocal strain gradient theory. *Int J Mech Sci* 156:31–45
66. Shiva K, Raghu P, Rajagopal A et al (2019) Nonlocal buckling analysis of laminated composite plates considering surface stress effects. *Compos Struct* 226:111216
67. Mondal S, Ramachandra LS (2019) Stability and failure analyses of delaminated composite plates subjected to localized heating. *Compos Struct* 209:258–267
68. Magnucki K, Witkowski D, Magnucka-Blandzi E (2019) Buckling and free vibrations of rectangular plates with symmetrically varying mechanical properties-Analytical and FEM studies. *Compos Struct* 220:355–361
69. Arefi M, Bidgoli EMR, Rabczuk T (2019) Effect of various characteristics of graphene nanoplatelets on thermal buckling behavior of FGRC micro plate based on MCST. *Eur J Mech A/Solids* 77:103802
70. Fu G, Zhou S, Qi L (2019) The size-dependent static bending of a partially covered laminated microbeam. *Int J Mech Sci* 152:411–419
71. Ji X, Li A, Zhou S (2017) A comparison of strain gradient theories with applications to the functionally graded circular micro-plate. *Appl Math Model* 49:124–143
72. Yang Y, Li XF (2019) Bending and free vibration of a circular magneto-electroelastic plate with surface effects. *Int J Mech Sci* 157:858–871
73. Ansari R, Gholami R, Shojaei MF et al (2015) Bending, buckling and free vibration analysis of size-dependent functionally graded circular/annular microplates based on the modified strain gradient elasticity theory. *Eur J Mech A/Solids* 49:251–267
74. Wang S, Kan J, Wang B et al (2013) Modeling and simulation of a piezodisc generator under central load. *Int J Appl Electromagnet Mech* 41(4):349–360

Publisher's Note Springer Nature remains neutral with regard to jurisdictional claims in published maps and institutional affiliations.